Research Square

Preprints are preliminary reports that have not undergone peer review.
They should not be considered conclusive, used to inform clinical practice,
or referenced by the media as validated information.

Bautin Bifurcation Analysis in a Filippov System Modeling the Interaction Between Pseudomonas aeruginosa and Host Immunity

Zhonghua Zhang

wwwzhangzhonghua@163.com

Yinuo Wang

Danning Zhang

Research Article

Keywords:

Posted Date: November 19th, 2026

DOI: https://doi.org/10.21203/rs.3.rs-11552154/v1

License: This work is licensed under a Creative Commons Attribution 4.0 International License.
Read Full License

Additional Declarations: No competing interests reported.

Bautin Bifurcation Analysis in a Filippov System Modeling the Interaction Between *Pseudomonas aeruginosa* and Host Immunity

Zhonghua Zhang* Yinuo Wang Danning Zhang

College of Science, Xi'an University of Science and Technology, Xi'an, Shaanxi, 710054, China

Faculty of Data Science, City University of Macau, Macau, 999078, China

*Corresponding author. E-mail: wwwzhangzhonghua@163.com

This work was not supported by any funding.

Abstract

When quorum sensing, a high density of pathogens accumulates within the host's local tissues, imposing immense pressure on the immune system and thereby eliciting complex host responses. Based on the Interaction between *Pseudomonas aeruginosa* and immune system of host, this paper proposes a discontinuous quorum sensing regulatory function that depends on bacterial concentration and establishes a four dimensional dynamical model describing the interactions among *Pseudomonas aeruginosa* population, quorum sensing signal molecules, cytokine IL 14, and human immune B cells. By applying the qualitative theory of differential equations and the theory of Filippov differential inclusions, we analyze the existence and stability of all possible equilibria, derive the criteria for the occurrence of Hopf and Bautin bifurcations and establish conditions for the existence of exactly one limit cycle, exactly two limit cycles, or a limit cycle of multiplicity greater than one. Furthermore, sensitivity analysis indicates that an enhanced immune clearance rate suppresses quorum sensing and bacterial population oscillations in the system, whereas an increased bacterial proliferation rate or strengthened quorum sensing activity increases the long term bacterial burden and amplifies oscillatory dynamics. The theoretical and numerical results obtained in this paper provide an important reference for further clarifying the mechanism of quorum sensing in *Pseudomonas aeruginosa* and for developing therapeutic schemes targeting the mutual regulatory threshold between pathogens and the immune system.

Keywords: Quorum sensing, Filippov system, Threshold, Hopf bifurcation, Bautin bifurcation

1 Introduction

Pseudomonas aeruginosa is a clinically important opportunistic pathogen in infection prevention and control. Its colonization and expansion are closely

related to the occurrence and development of chronic respiratory infections, infections in immunocompromised hosts, and healthcare associated infections. Recent studies[1,2] have confirmed that *Pseudomonas aeruginosa* can sense bacterial density through signal molecules secreted by itself and coordinate bacterial group behavior accordingly. This regulatory mechanism is defined as quorum sensing (QS). The QS system can change the activation level of the host immune system through accumulated signal molecules. As bacterial density increases, QS signal molecules induce the host immune system to secrete the cytokine IL 14 and activate B cells. Through IL 14 mediated inflammatory responses together with B cell mediated specific clearance, the host immune system regulates bacterial colonization and expansion in vivo[3,4].

Many studies have investigated the dynamics by which QS mechanisms regulate the interaction between bacteria and the host immune system. Telford et al.[5] found that QS signal molecules of *Pseudomonas aeruginosa* can directly modulate immunity by inhibiting lymphocyte proliferation and reducing TNF α release from macrophages. This indicates that, in addition to regulating bacterial virulence, the QS signal molecule affects clearance of infection by suppressing pro inflammatory factors, altering the Th1/Th2 balance, and regulating B cell antibody responses. Experimental studies by Smith et al.[6] and Bortolotti et al.[7] confirmed that QS signal molecules of *Pseudomonas aeruginosa* can activate T cells to produce the cytokine IL 14, thereby promoting B cell proliferation and mediating adaptive immune responses.

In addition to experimental investigations, some scholars have established dynamical models to systematically elucidate the regulatory laws of QS mechanisms in the interactions between pathogens and the host immune system. Fergola et al.[8] developed an ordinary differential equation model of bacteria immune competition with and without QS. Their results showed that bacterial elimination or coexistence with immune cells is determined by a threshold parameter, while QS can alter equilibrium stability and thus change the outcome of bacteria immune competition. For the early stage of *Pseudomonas aeruginosa* burn wound infection, Koerber et al.[9] developed a mathematical model including bacterial proliferation, diffusion of QS signal molecules, and regulation of virulence factor expression. The model revealed that *Pseudomonas aeruginosa* populations can enhance virulence factor expression through density dependent QS activation and alter the relationship between local bacterial load and host immune response. Ward et al.[10] developed a differential equation model for bacterial proliferation and QS regulation. They found a threshold-like transition in QS activation and a unique biologically meaningful steady state that is linearly stable, providing a dynamical explanation for density-dependent quorum sensing. Zhang et al.[11] developed a periodic bacteria-immunity model incorporating time-delayed quorum sensing mechanisms to characterize the competitive interactions between bacterial populations and host immune cells, and systematically investigated the existence, stability of the positive periodic solutions, as well as the emergence of subharmonic bifurcations.

The studies [8–11] used continuous dynamical models to investigate the regulation of bacterial QS mechanisms on various physiological behaviors of the host,

providing a theoretical basis for understanding QS occurrence, virulence factor expression, host immune response, and other physiological processes. However, from the physiological mechanism of bacterial QS, when the bacterial concentration reaches the QS activation threshold, the bacterial load in local host tissues rises rapidly, and the intensity of the confrontation between the bacterial population and the immune system increases sharply. Such stepwise transitions are difficult to describe accurately with continuous models.

To date, substantial progress has been made in the dynamical study of discontinuous systems for infectious diseases. To capture threshold-induced changes that are difficult to describe using continuous models, two-dimensional discontinuous systems have been increasingly employed in the study of epidemic dynamics. For example, Wang and Xiao[12] formulated a two-dimensional Filippov epidemic model with a piecewise-continuous transmission rate to characterize abrupt changes in disease transmission induced by intervention measures once a prescribed threshold is reached. They analyzed the sliding dynamics on the switching manifold, established the existence and stability of different types of equilibria, and investigated nonsmooth dynamical phenomena, including threshold-induced sliding bifurcations. Based on a SIR epidemic model, Guo et al.[13] discussed in detail the existence and stability of various equilibria and found that discontinuous treatment strategies can significantly change disease dynamics and, under certain conditions, accelerate the decline of infected individuals and disease control. Starting from a threshold regulation mechanism induced by selection pressure, Qin and Tang[14] established a discontinuous epidemic model and discussed the existence and stability of various equilibria and the properties of local bifurcations induced by threshold switching. Their results revealed that models under discontinuous selection pressure regulation may exhibit nonsmooth dynamical behaviors. Chong et al.[15] formulated a Filippov model incorporating a discontinuous threshold control strategy, where the threshold is determined by the number of poultry infected with avian influenza. They found that threshold strategies can induce a bistable mechanism involving disease elimination and endemic coexistence. Carvalho et al.[16] established a discontinuous epidemic model for COVID-19. They found that discontinuous interventions can trigger intermittent oscillatory outbreaks near the healthcare capacity threshold. In summary, the switching manifold plays a central role in threshold-controlled epidemic systems. It may induce sliding motion, pseudo-equilibria, and nonsmooth bifurcations, thereby significantly affecting disease persistence, outbreak patterns, and the effectiveness of control strategies. Similar studies can be found in [17–19].

It can be seen that [12–19] all used two dimensional Filippov systems to describe discontinuous dynamical characteristics in the transmission of infectious diseases. However, the interaction between bacterial quorum sensing and human immune system involves complex physiological regulatory processes, two dimensional Filippov systems cannot accurately characterize complex biological and physiological processes among the competition. It is therefore reasonable to develop higher dimensional discontinuous models to characterize these interactions. But as the dimension of a Filippov system increases, the dy-

namics in each high-dimensional subregion divided by switching manifold become more complex, while the switching manifold changes from a line in a two-dimensional phase space to a hypersurface in a higher-dimensional phase space. Consequently,the sliding-mode dynamics on the switching manifold, together with the collision patterns between the trajectories originating in the two subregions and the sliding motion, become exceptionally complex.Encouragingly, in the field of infectious disease dynamics, some scholars have conducted exploratory researches on three-dimensional discontinuous models. Zhou and Tang[20] formulated a Filippov system featuring a two-dimensional switching manifold defined over a three-dimensional phase space, and performed a rigorous theoretical analysis on the existence and stability of pseudo-equilibria on the sliding manifold, as well as the non-smooth bifurcation behaviors induced by threshold-mediated switching. To describe the effect of limited medical resources on disease transmission, Dong et al.[21] established a three dimensional Filippov epidemic model with a discontinuous treatment strategy. They systematically analyzed the subsystem and the sliding mode dynamics on the two dimensional switching surface, derived criteria for saddle node bifurcation,transcritical bifurcation and boundary equilibrium bifurcation, and found that medical resource constraints can cause bistable dynamics involving coexistence of endemic equilibria and pseudo equilibria. It can be concluded from the aforementioned studies that the high-dimensional switching manifold in high-dimensional non-smooth systems can not only accurately characterize the threshold-type transition regulatory effect of therapeutic intervention strategies, but also drive the system to evolve complex and diverse global dynamical behaviors.

In this paper, we introduce a discontinuous function to describe the stepwise change in *Pseudomonas aeruginosa* concentration within the host upon the onset of QS, and formulate a four dimensional Filippov system driven by QS behavior to characterize the interactions among *Pseudomonas aeruginosa*, QS signal molecules, adaptive immune B cells, and T cell cytokine IL-14. At the same time, the qualitative theory of differential equations and the theory of Filippov differential inclusions are used to analyze the existence and stability of all kinds of equilibria, as well as the conditions for occurrence and properties of the branches of Hopf and Bautin bifurcations. Sensitivity analysis identifies key parameters affecting long term bacterial load, duration of QS activation, bacterial oscillation intensity, and host immune response level. This study systematically reveals the dynamical evolution law of *Pseudomonas aeruginosa* infection mediated by QS threshold regulation and provides a theoretical basis for the prevention and clinical treatment of *Pseudomonas aeruginosa* infectious diseases such as chronic respiratory infections, infections in immunocompromised hosts, healthcare associated infections, and burn wound infections.

2 Model Formulation

Let $P(t), Q(t), X(t), B(t)$ denote, respectively, the concentration of *Pseudomonas aeruginosa* in local tissue of the host, the concentration of QS signal

molecules by *Pseudomonas aeruginosa*, the concentration of the cytokine IL 14, and the concentration of B cells at time t.

Assume that the *Pseudomonas aeruginosa* population grows in host according to the logistic function $rP(1-P/K)$, where r is the intrinsic growth rate and K is the environmental carrying capacity. The *Pseudomonas aeruginosa* population releases QS signal molecules at rate m, and the QS signal molecules degrade at rate d_0. When the bacterial concentration exceeds the threshold P_a, quorum sensing is activated, bacterial group behavior is enhanced, and the host immune response is further affected. Specifically, the QS signal molecules induce the host to produce the T cell factor IL 14 at rate β_1, promote activation and proliferation of B cells at rate β_2, and decay naturally at rate d_1. The intrinsic proliferation rate of B cells in the host is α; B cells clear *Pseudomonas aeruginosa* at rate δ, and B cells themselves decay naturally at rate d_2. The above mechanism is illustrated in Figure 1.

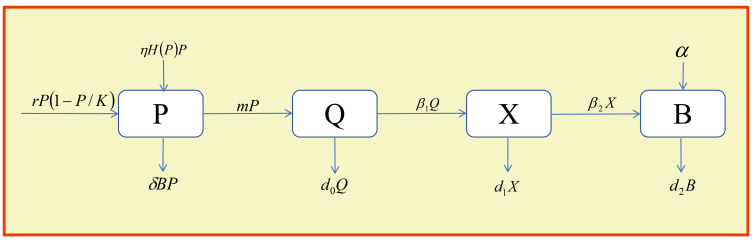


Figure 1: Compartment diagram.

Based on the above assumptions, the following four dimensional nonsmooth dynamical system is

$$\begin{cases} \dfrac{\mathrm{d}P}{\mathrm{d}t} = rP\left(1-\dfrac{P}{K}\right) + \eta H(P)P - \delta BP, \\ \dfrac{\mathrm{d}Q}{\mathrm{d}t} = mP - d_0 Q, \\ \dfrac{\mathrm{d}X}{\mathrm{d}t} = \beta_1 Q - d_1 X, \\ \dfrac{\mathrm{d}B}{\mathrm{d}t} = \alpha + \beta_2 X - d_2 B. \end{cases} \tag{1}$$

Here $H(P)$ is the step function of the quorum sensing threshold, with expression

$$H(P) = \begin{cases} 0, & P < P_a, \\ 1, & P > P_a. \end{cases}$$

Thus, when $P < P_a$, the *Pseudomonas aeruginosa* concentration is low and QS does not occur; when $P > P_a$, the *Pseudomonas aeruginosa* concentration is high and QS occurs.

3 Stability Analysis

3.1 Existence of equilibria

Define the low bacterial load domain and the high bacterial load domain as

$$\Omega_1 = \{(P, Q, X, B) \in \mathbb{R}^4_+ \mid P < P_a\}, \Omega_2 = \{(P, Q, X, B) \in \mathbb{R}^4_+ \mid P > P_a\}.$$

Lemma 3.1 For any nonnegative initial condition $(P(0), Q(0), X(0), B(0)) \in \mathbb{R}^4_+$, the solution of system (1) remains nonnegative for all $t \geq 0$, and all variables in system (1) are bounded.

Proof We first prove nonnegativity. Integrating the first equation of system (1) yields

$$P(t) = P(0) \exp\left\{\int_0^t \left[r\left(1 - \frac{P(s)}{K}\right) + \eta H(P(s)) - \delta B(s)\right] \mathrm{d}s\right\} \geq 0.$$

Similarly, one can prove successively that $Q(t) \geq 0$, $X(t) \geq 0$, and $B(t) \geq 0$.

We next prove boundednessof the solutions to system (1). Since $H(P) \leq 1$ and $B, P \geq 0$, we have

$$\begin{aligned}\frac{\mathrm{d}P(t)}{\mathrm{d}t} &= rP(t)\left(1 - \frac{P(t)}{K}\right) + \eta H(P(t))P(t) - \delta B(t)P(t) \\ &\leq rP(t)\left(1 - \frac{P(t)}{K}\right) + \eta P(t).\end{aligned}$$

By the properties of the Bernoulli equation,

$$P(t) \leq M_P,$$

where $M_P = \max\left\{P(0), K\left(1 + \frac{\eta}{r}\right)\right\}$. From the second equation of system (1),

$$\frac{\mathrm{d}Q}{\mathrm{d}t} \leq mM_P - d_0 Q,$$

and therefore

$$Q(t) \leq \max\left\{Q(0), \frac{mM_P}{d_0}\right\}.$$

Likewise, $X(t)$ and $B(t)$ are bounded.

For convenience, define threshold parameters

$$R_{01} = \frac{rd_2}{\delta\alpha}, \quad R_{02} = \frac{(r+\eta)d_2}{\delta\alpha},$$

and

$$R_{0a} = 1 + \left(\frac{rd_2}{K\delta\alpha} + \frac{\beta_1\beta_2 m}{\alpha d_0 d_1}\right) P_a.$$

Theorem 3.1 The following conclusions hold for the existence of equilibria of system (1):System (1) always has the bacteria free equilibrium $E_0 =$

$\left(0,0,0,\frac{\alpha}{d_2}\right)$. If $R_{01}>1$, system (1) has a low bacterial load positive equilibrium $E_1=(P_1^*,Q_1^*,X_1^*,B_1^*)$; If $R_{02}>1$, system (1) has a high bacterial load positive equilibrium $E_2=(P_2^*,Q_2^*,X_2^*,B_2^*)$,where

$$P_i^*=\frac{\delta\alpha}{d_2(c_1+c_2)}(R_{0i}-1),\quad Q_i^*=\frac{mP_i^*}{d_0},\quad X_i^*=\frac{\beta_1 mP_i^*}{d_0d_1},\quad B_i^*=\frac{\alpha d_0d_1+\beta_1\beta_2 mP_i^*}{d_0d_1d_2},$$
$$c_1=\frac{r}{K},\quad c_2=\frac{\delta\beta_1\beta_2 m}{d_0d_1d_2}.$$

Proof The bacteria free equilibrium $E_0=(0,0,0,\alpha/d_2)$ evidently exists. Next, we discuss the existence of positive equilibria. Setting the right hand side of system (1) equal to zero and solving the algebraic equations gives

$$Q=\frac{mP}{d_0},\quad X=\frac{\beta_1 mP}{d_0d_1},\quad B=\frac{\alpha d_0d_1+\beta_1\beta_2 mP}{d_0d_1d_2},$$

where P satisfies the algebraic equation

$$r\left(1-\frac{P}{K}\right)+\eta H(P)-\frac{\delta}{d_0d_1d_2}\left(\alpha d_0d_1+\beta_1\beta_2 mP\right)=0. \tag{2}$$

We now discuss the existence of nonnegative solutions of Eq.(2).

When $P<P_a$, Eq.(2) reduces to

$$r\left(1-\frac{P}{K}\right)-\frac{\delta}{d_0d_1d_2}\left(\alpha d_0d_1+\beta_1\beta_2 mP\right)=0.$$

Solving gives

$$P=\frac{rKd_0d_1d_2-\delta K\alpha d_0d_1}{rd_0d_1d_2+\delta h}=\frac{\delta\alpha}{d_2(c_1+c_2)}(R_{01}-1):=P_1^*.$$

If $R_{01}>1$, we have $P_1^*>0$, so system (1) has the positive equilibrium E_1 in the low bacterial load domain. When $P>P_a$, Eq.(2) reduces to

$$r\left(1-\frac{P}{K}\right)+\eta-\frac{\delta}{d_0d_1d_2}\left(\alpha d_0d_1+\beta_1\beta_2 mP\right)=0.$$

Solving gives

$$P=\frac{(r+\eta)Kd_0d_1d_2-\delta K\alpha d_0d_1}{rd_0d_1d_2+\delta h}=\frac{\delta\alpha}{d_2(c_1+c_2)}(R_{02}-1):=P_2^*.$$

If $R_{02}>1$, we have $P_2^*>0$, so system (1) has the positive equilibrium E_2 in the high bacterial load domain.

Remarks: If $1<R_{01}<R_{0a}$, system (1) has the low bacterial load positive (real) equilibrium E_1; if $R_{0a}<R_{02}$, system (1) has the high bacterial load positive (real) equilibrium E_2 and if $1<R_{01}<R_{0a}<R_{02}$, then both E_1 and E_2 are positive (real) equilibria and coexist.

3.2 Stability of equilibria

For computational simplicity, let

$$s_i = r \prod_{0\le p<q\le 2}(d_p+d_q)\prod_{k=0}^{2}[d_k + L(R_{0i}-1)] - \delta h L(R_{0i}-1)\left[L(R_{0i}-1)+d_0+d_1+d_2\right]^2,$$

where

$$L = \frac{r d_0 d_1 \delta\alpha}{r d_0 d_1 d_2 + \delta h}, \quad h = K\beta_1\beta_2 m, \quad i = 1, 2.$$

Theorem 3.2 The following hold for the stability of the equilibria E_0, E_1, and E_2 of system (1): If $R_{01} < 1$, the bacteria free equilibrium E_0 is locally asymptotically stable, whereas if $R_{01} > 1$, it is unstable; If $1 < R_{01} < R_{0a}$ and $s_1 > 0$, the low bacterial load positive equilibrium E_1 is locally asymptotically stable; And if $R_{0a} < R_{02}$ and $s_2 > 0$, the high bacterial load positive equilibrium E_2 is locally asymptotically stable.

Proof The eigenvalues of the Jacobian matrix of the system (1) at E_0 are

$$\lambda_1 = \frac{\delta\alpha}{d_2}(R_{01}-1), \quad \lambda_2 = -d_0 < 0, \quad \lambda_3 = -d_1 < 0, \quad \lambda_4 = -d_2 < 0.$$

Therefore, when $R_{01} < 1$, the bacteria free equilibrium E_0 is locally asymptotically stable; when $R_{01} > 1$, it is unstable.

For the positive equilibrium E_i, the characteristic equation is

$$\lambda^4 + a_1^i\lambda^3 + a_2^i\lambda^2 + a_3^i\lambda + a_4^i = 0, \tag{3}$$

where

$$a_1^i = \frac{rP_i^*}{K} + d_0 + d_1 + d_2, a_2^i = \frac{rP_i^*}{K}(d_0+d_1+d_2) + d_0d_1 + d_0d_2 + d_1d_2,$$
$$a_3^i = \frac{rP_i^*}{K}(d_0d_1 + d_0d_2 + d_1d_2) + d_0d_1d_2, a_4^i = \frac{rP_i^*}{K}d_0d_1d_2 + \delta m\beta_1\beta_2 P_i^*.$$

By the Hurwitz criterion, E_i is locally asymptotically stable if and only if all leading principal minors $\Delta_j^i, j = 1, 2, 3, 4$ of the Hurwitz matrix are positive. Since $a_1^i, a_2^i, a_3^i, a_4^i > 0$ and

$$\begin{aligned}
\Delta_1^i &= a_1^i > 0,\\
\Delta_2^i &= a_1^i a_2^i - a_3^i\\
&= (d_0+d_1)(d_0+d_2)(d_1+d_2) + \frac{rP_i^{*2}}{K^2}(d_0+d_1+d_2) > 0,\\
\Delta_3^i &= a_1^i a_2^i a_3^i - (a_1^i)^2 a_4^i - (a_3^i)^2\\
&= r\prod_{0\le p<q\le 2}(d_p+d_q)\prod_{k=0}^{2}[d_k + L(R_{0i}-1)]\\
&\quad - \delta h L(R_{0i}-1)\left[L(R_{0i}-1)+d_0+d_1+d_2\right]^2,\\
\Delta_4^i &= a_4^i\Delta_3^i,
\end{aligned}$$

it follows that when $R_{0i} > 1$ and $s_i > 0$, the positive equilibrium E_i is locally asymptotically stable.

We next study the global asymptotic stability of equilibria.

Theorem 3.3 If $R_{01} < 1$, the bacteria free equilibrium E_0 is globally asymptotically stable.

Proof Since the bacteria free equilibrium E_0 is locally asymptotically stable, next, we prove the global attractivity.

We first prove $\lim\limits_{t\to\infty} P(t) = 0$. If $P(0) = 0$, then the first equation of system (1) gives $P(t) \equiv 0$. Consider the next case $P(0) > 0$. By **Lemma 3.1**, when $P(0) > 0$, we have $P(t) > 0$ for any $t \geq 0$, and hence

$$\frac{\mathrm{d}}{\mathrm{d}t} \ln P(t) = r\left(1 - \frac{P(t)}{K}\right) - \delta B(t) \leq r - \delta B(t).$$

From the fourth equation of system (1),

$$\begin{aligned} B(t) &= B(0)e^{-d_2 t} + \int_0^t e^{-d_2(t-s)} \left(\alpha + \beta_2 X(s)\right) \mathrm{d}s \\ &= \frac{\alpha}{d_2} + \left(B(0) - \frac{\alpha}{d_2}\right) e^{-d_2 t} + \beta_2 \int_0^t e^{-d_2(t-s)} X(s) \mathrm{d}s. \end{aligned}$$

By **Lemma 3.1**, the nonnegative orthant $\mathbb{R}^4_+$ is positively invariant under system (1), $X(t) \geq 0$, so

$$B(t) \geq \frac{\alpha}{d_2} + \left(B(0) - \frac{\alpha}{d_2}\right) e^{-d_2 t}.$$

Therefore,

$$\frac{\mathrm{d}}{\mathrm{d}t} \ln P(t) \leq (R_{01} - 1) - \delta \left(B(0) - \frac{\alpha}{d_2}\right) e^{-d_2 t}.$$

Integrating both sides from 0 to t gives

$$\begin{aligned} \ln \frac{P(t)}{P(0)} &\leq (R_{01} - 1)t - \delta \left(B(0) - \frac{\alpha}{d_2}\right) \int_0^t e^{-d_2 s} \mathrm{d}s \\ &= (R_{01} - 1)t - \delta \left(B(0) - \frac{\alpha}{d_2}\right) (1 - e^{-d_2 t}). \end{aligned}$$

Thus

$$P(t) \leq P(0) \exp\left\{(R_{01} - 1)t - \delta \left(B(0) - \frac{\alpha}{d_2}\right) (1 - e^{-d_2 t})\right\}.$$

The above expression shows that $P(t)$ converges exponentially to zero if $R_{01} < 1$. Therefore, when $R_{01} < 1$,

$$\lim_{t\to\infty} P(t) = 0.$$

Similarly,

$$\lim_{t\to\infty} Q(t) = 0, \quad \lim_{t\to\infty} X(t) = 0, \quad \lim_{t\to\infty} B(t) = \frac{\alpha}{d_2}.$$

Hence, when $R_{01} < 1$, the bacteria free equilibrium E_0 is globally asymptotically stable.

Theorem 3.4 If $1 < R_{01} < R_{0a}$ and $4c_1 > c_2$, then the low bacterial load positive equilibrium E_1 is asymptotically stable in Ω_1.

Proof Let $u = P - P_1^*$, $v = Q - Q_1^*$, $y = X - X_1^*$, and $w = B - B_1^*$. Construct the Lyapunov function

$$V = P - P_1^* - P_1^* \ln \frac{P}{P_1^*} + \frac{a_1}{2}v^2 + \frac{a_2}{2}y^2 + \frac{a_3}{2}w^2,$$

where $a_1, a_2, a_3 > 0$ are to be determined. Since $x - 1 - \ln x \geq 0$ for any $x > 0$, with equality if and only if $x = 1$, we have $V \geq 0$. The derivative of V along trajectories of system (1) is

$$\frac{\mathrm{d}V}{\mathrm{d}t} = -\frac{r}{K}u^2 - a_1 d_0 v^2 - a_2 d_1 y^2 - a_3 d_2 w^2 + a_1 muv + a_2\beta_1 vy + a_3\beta_2 yw - \delta uw.$$

Writing this as a quadratic form gives

$$\frac{\mathrm{d}V}{\mathrm{d}t} = -(u, v, y, w)M(u, v, y, w)^T,$$

where

$$M = \begin{pmatrix} \frac{r}{K} & -\frac{a_1 m}{2} & 0 & \frac{\delta}{2} \\ -\frac{a_1 m}{2} & a_1 d_0 & -\frac{a_2\beta_1}{2} & 0 \\ 0 & -\frac{a_2\beta_1}{2} & a_2 d_1 & -\frac{a_3\beta_2}{2} \\ \frac{\delta}{2} & 0 & -\frac{a_3\beta_2}{2} & a_3 d_2 \end{pmatrix}.$$

Thus, to prove that $\mathrm{d}V/\mathrm{d}t$ is negative definite, it suffices to prove that M is positive definite. Take

$$a_1 = \frac{n^2 r d_0}{m^2 K}, \quad a_2 = \frac{n^4 r d_0^2 d_1}{m^2 K \beta_1^2}, \quad a_3 = \frac{n^6 r d_0^2 d_1^2 d_2}{m^2 K \beta_1^2 \beta_2^2},$$

where

$$n = \left(\frac{K\delta m\beta_1\beta_2}{r d_0 d_1 d_2}\right)^{1/4}.$$

Let Λ_i be the leading principal minors of M, $i = 1, 2, 3, 4$. Direct calculation gives

$$\Lambda_1 = \frac{r}{K} > 0, \quad \Lambda_2 = \frac{d_0^2 r^2}{4K^2 m^2} n^2(4 - n^2), \quad \Lambda_3 = \frac{d_0^4 d_1^2 r^3}{2K^3\beta_1^2 m^4} n^6(2 - n^2),$$

$$\Lambda_4 = \frac{d_0^6 d_1^4 d_2^2 r^4}{4K^4\beta_1^4\beta_2^2 m^6} n^{12}(2 - n^2)^2 > 0.$$

Hence, if $0 < n^2 < 2$, that is, if $4c_1 > c_2$, the leading principal minors satisfy $\Lambda_i > 0$ for $i = 1, 2, 3, 4$, and the matrix M is positive definite. Therefore, if

$1 < R_{01} < R_{0a}$ and $4c_1 > c_2$, the low bacterial load positive equilibrium E_1 is asymptotically stable in Ω_1.

Similarly, the asymptotic stability of the high bacterial load positive equilibrium E_2 in Ω_2 can be discussed.

Theorem 3.5 If $R_{02} > R_{0a}$ and $4c_1 > c_2$, then the high bacterial load positive equilibrium E_2 is asymptotically stable in Ω_2.

Corollary 3.1 If $1 < R_{01} < R_{0a} < R_{02}$ and $4c_1 > c_2$, then system (1) exhibits bistable dynamical behavior.

We further proceed to investigate the potential Hopf bifurcation phenomena occurring at the positive equilibria of the system (1). To this end, we take the intrinsic growth rate r as the bifurcation parameter and suppose that the characteristic equation has purely imaginary roots $\lambda = \pm \mathrm{i}\omega_i$,where i is the imaginary unit and $\omega_i > 0$. Substituting it into the Eq.(3) yields

$$\omega_i^4 \mp \mathrm{i}a_1^i(r)\omega_i^3 - a_2^i(r)\omega_i^2 \pm \mathrm{i}a_3^i(r)\omega_i + a_4^i(r) = 0.$$

Separating the real and imaginary parts gives

$$\begin{cases} \omega_i^4 - a_2^i(r)\omega_i^2 + a_4^i(r) = 0, \\ a_3^i(r)\omega_i - a_1^i(r)\omega_i^3 = 0. \end{cases}$$

Thus $\omega_i^2 = a_3^i(r)/a_1^i(r)$. Substituting this into the first equation gives

$$\frac{A_3^i r^3 + A_2^i r^2 + A_1^i r + A_0^i}{(rd_0d_1d_2 + \delta K\beta_1\beta_2 m)^3 \left(\frac{rP_i^*}{K} + d_0 + d_1 + d_2\right)^2} = 0,$$

where

$$\begin{aligned}
A_3^i &= (d_0d_1)^3 \prod_{0\le j<k\le 2}(d_j + d_k) \prod_{p=0}^{2} \left[d_p d_2 + \delta\alpha(R_{0i} - 1)\right], \\
A_2^i &= \delta h(d_0d_1)^2 \Bigg(\prod_{0\le j<k\le 2}(d_j + d_k) \sum_{p=0}^{2} d_p \prod_{\substack{q=0 \\ q\ne p}}^{2} \left[d_q d_2 + \delta\alpha(R_{0i} - 1)\right] \\
&\qquad - d_0d_1\delta\alpha(R_{0i} - 1)\left[d_2\tau + \delta\alpha(R_{0i} - 1)\right]^2 \Bigg), \\
A_1^i &= (\delta h)^2 d_0d_1 \Bigg(\prod_{0\le j<k\le 2}(d_j + d_k) \sum_{p=0}^{2} \prod_{\substack{q=0 \\ q\ne p}}^{2} d_q \left[d_p d_2 + \delta\alpha(R_{0i} - 1)\right] \\
&\qquad - 2d_0d_1\delta\alpha(R_{0i} - 1)\tau\left[d_2\tau + \delta\alpha(R_{0i} - 1)\right] \Bigg), \\
A_0^i &= (\delta h)^3 d_0d_1 \left(d_2 \prod_{0\le j<k\le 2}(d_j + d_k)^2 - \delta\alpha(R_{0i} - 1)\tau \right), \\
\tau &= d_0 + d_1 + d_2.
\end{aligned}$$

For convenience of discussion, let the numerator of the above fraction be denoted by $F_i(r)$.

Lemma 3.2 If $r^i > 0$ is a positive root of $F_i(r) = 0$, then it is simple.

Proof Suppose to the contrary, that $r^i > 0$ is a multiple root of $F_i(r) = 0$. Then we have $F_i(r^i) = 0$ and $F_i'(r^i) = 0$. Since F_i is a cubic polynomial and r^i is a multiple root, there exists a real number v such that

$$F_i(r) = A_3^i(r - r^i)^2(r - v).$$

Expanding the right-hand side yields

$$F_i(r) = A_3^i\Big[r^3 - (2r^i + v)r^2 + \big((r^i)^2 + 2r^i v\big)r - (r^i)^2 v\Big].$$

Comparing with the expression of $F_i(r)$ yields,

$$A_2^i = -A_3^i(2r^i + v), A_1^i = A_3^i\big[(r^i)^2 + 2r^i v\big], A_0^i = -A_3^i(r^i)^2 v.$$

Since $A_0^i < 0$, $A_3^i > 0$, and $r^i > 0$, the last equality implies that $v > 0$. Consequently,

$$A_2^i < 0, \quad A_1^i > 0.$$

On the other hand, $A_2^i < 0$ implies

$$\prod_{0\le j<k\le 2}(d_j+d_k)^2 \sum_{p=0}^{2} d_p \prod_{\substack{q=0\\ q\neq p}}^{2} [d_q d_2 + \delta\alpha(R_{0i} - 1)] < d_0 d_1 \delta\alpha(R_{0i}-1)\left[d_2\tau + \delta\alpha(R_{0i} - 1)\right]^2. \tag{4}$$

To derive a contradiction, write

$$A_1^i = (\delta K\beta_1\beta_2 m)^2 d_0 d_1 G,$$

where

$$\begin{aligned} G = &\prod_{0\le j<k\le 2}(d_j + d_k)^2 \sum_{p=0}^{2}\prod_{\substack{q=0\\ q\neq p}}^{2} d_q \left[d_p d_2 + \delta\alpha(R_{0i} - 1)\right] \\ &- 2d_0 d_1 \delta\alpha(R_{0i} - 1)\left[d_2\tau + \delta\alpha(R_{0i} - 1)\right]. \end{aligned}$$

Since

$$\begin{aligned} &2\tau\sum_{p=0}^{2} d_p \prod_{\substack{q=0\\ q\neq p}}^{2} [d_q d_2 + \delta\alpha(R_{0i} - 1)] - [d_2\tau + \delta\alpha(R_{0i} - 1)] \sum_{p=0}^{2}\prod_{\substack{q=0\\ q\neq p}}^{2} d_q \ \ [d_p d_2 + \delta\alpha(R_{0i} - 1)] \\ &= 2d_0^2[\delta\alpha(R_{0i} - 1)]^2 + 3d_0 d_1[\delta\alpha(R_{0i} - 1)]^2 + 3d_0 d_2[\delta\alpha(R_{0i} - 1)]^2 \\ &\quad + 2d_1^2[\delta\alpha(R_{0i} - 1)]^2 + 3d_1 d_2[\delta\alpha(R_{0i} - 1)]^2 + 2d_2^2[\delta\alpha(R_{0i} - 1)]^2 \\ &\quad + 3d_0^2 d_1 d_2\delta\alpha(R_{0i} - 1) + 3d_0^2 d_2^2\delta\alpha(R_{0i} - 1) + 3d_0 d_1^2 d_2\delta\alpha(R_{0i} - 1) \\ &\quad + 6d_0 d_1 d_2^2\delta\alpha(R_{0i} - 1) + 3d_0 d_2^3\delta\alpha(R_{0i} - 1) + 3d_1^2 d_2^2\delta\alpha(R_{0i} - 1) \\ &\quad + 3d_1 d_2^3\delta\alpha(R_{0i} - 1) + 3d_0^2 d_1 d_2^3 + 3d_0 d_1^2 d_2^3 + 3d_0 d_1 d_2^4 > 0, \end{aligned}$$

we have

$$2\tau\sum_{p=0}^{2} d_p \prod_{\substack{q=0\\q\neq p}}^{2} \left[d_q d_2 + \delta\alpha\left(R_{0i}-1\right)\right] > \left[d_2\tau + \delta\alpha\left(R_{0i}-1\right)\right]\sum_{p=0}^{2}\prod_{\substack{q=0\\q\neq p}}^{2} d_q\left[d_p d_2 + \delta\alpha\left(R_{0i}-1\right)\right].$$

Multiplying both sides of the above equation by $\prod_{0\leq j<k\leq 2}(d_j+d_k)^2$ and combining with inequality (4), one obtains

$$\begin{aligned}
&\prod_{0\leq j<k\leq 2}(d_j+d_k)^2\sum_{p=0}^{2}\prod_{\substack{q=0\\q\neq p}}^{2} d_q\ \left[d_p d_2 + \delta\alpha(R_{0i}-1)\right]\\
&\quad< \frac{2\tau}{d_2\tau+\delta\alpha(R_{0i}-1)}\prod_{0\leq j<k\leq 2}(d_j+d_k)^2\sum_{p=0}^{2} d_p\prod_{\substack{q=0\\q\neq p}}^{2}\left[d_q d_2+\delta\alpha(R_{0i}-1)\right]\\
&\quad< \frac{2\tau}{d_2\tau+\delta\alpha(R_{0i}-1)} d_0 d_1\delta\alpha(R_{0i}-1)\left[d_2\tau+\delta\alpha(R_{0i}-1)\right]^2\\
&\quad= 2d_0 d_1\delta\alpha(R_{0i}-1)\left[d_2\tau+\delta\alpha(R_{0i}-1)\right].
\end{aligned}$$

As a result, we obtain the inequality $G<0$, which stands in direct contradiction to the prior assumption $A_1^i>0$. It therefore follows that r^i is a simple root of the characteristic equation.

Theorem 3.6 If

$$R_{0i} > 1+\frac{d_2(d_0+d_1)^2(d_0+d_2)^2(d_1+d_2)^2}{\delta\alpha(d_0+d_1+d_2)},$$

then there exists $r=r_0^i$ such that $F_i(r_0^i)=0$ and $F_i'(r_0^i)\neq 0$. Consequently, system (1) undergoes a Hopf bifurcation at the equilibrium E_i.

Proof We show that there exists $r=r_0^i$ satisfying $F_i(r)=0$. When $R_{0i}>1$, $A_3^i>0$, so there exists a positive number r_0^i such that $F_i(r_0^i)>0$. If

$$R_{0i} > 1+\frac{d_2(d_0+d_1)^2(d_0+d_2)^2(d_1+d_2)^2}{\delta\alpha(d_0+d_1+d_2)},$$

then $A_0^i<0$ and hence $F_i(0)<0$. By the intermediate value theorem, a positive number r_0^i exists such that $F_i(r)=0$.

The transversality condition is verified as follows. Differentiating $F_i(r)$ gives

$$F_i'(r) = 3A_3^i r^2 + 2A_2^i r + A_1^i.$$

By **Lemma 3.2**, r_0^i is a sample root of $F_i(r)=0$. Thus $F_i'(r_0^i)\neq 0$. Hence the characteristic roots cross the imaginary axis with nonzero speed, and a Hopf bifurcation occurs.

To determine the type of Hopf bifurcation [23–25], denote the first Lyapunov coefficient by l_1^i. Let

$$u=P-P_i^*,\quad v=Q-Q_i^*,\quad x=X-X_i^*,\quad y=B-B_i^*.$$

The system can then be written as

$$Z' = M_i Z + \frac{1}{2}\left(-\frac{2r}{K}u^2 - 2\delta uy, 0, 0, 0\right)^T,$$

where

$$Z = (u, v, x, y)^T \in \mathbb{R}^4_+, M_i = \begin{pmatrix} -rP_i^*/K & 0 & 0 & -\delta P_i^* \\ m & -d_0 & 0 & 0 \\ 0 & \beta_1 & -d_1 & 0 \\ 0 & 0 & \beta_2 & -d_2 \end{pmatrix}.$$

Take the right eigenvector of M_i associated with eigenvalue $\mathrm{i}\omega_i$ as

$$q_i = \left(1, \frac{m}{d_0 + \mathrm{i}\omega_i}, \frac{m\beta_1}{(d_0 + \mathrm{i}\omega_i)(d_1 + \mathrm{i}\omega_i)}, \frac{m\beta_1\beta_2}{(d_0 + \mathrm{i}\omega_i)(d_1 + \mathrm{i}\omega_i)(d_2 + \mathrm{i}\omega_i)}\right)^T.$$

and the adjoint eigenvector of M_i^T associated with eigenvalue $-\mathrm{i}\omega_i$ as

$$\widetilde{p}_i = \left(1, -\frac{rP_i^* - \mathrm{i}\omega_i K}{mK}, \frac{(d_0 - \mathrm{i}\omega_i)(rP_i^* - \mathrm{i}\omega_i K)}{mK\beta_1}, \frac{(d_0 - \mathrm{i}\omega_i)(d_1 - \mathrm{i}\omega_i)(rP_i^* - \mathrm{i}\omega_i K)}{mK\beta_1\beta_2}\right)^T.$$

Define the complex inner product

$$\langle p_i, q_i\rangle = \overline{\widetilde{p_i}}^T q_i = 1 + \left(\frac{rP_i^*}{K} + \mathrm{i}\omega_i\right)\left(\frac{1}{d_0 + \mathrm{i}\omega_i} + \frac{1}{d_1 + \mathrm{i}\omega_i} + \frac{1}{d_2 + \mathrm{i}\omega_i}\right) := \Psi_i,$$

where $\overline{p_i}^T$ denotes the conjugate transpose of p_i.

For convenience, set $S = d_0 + d_1$, $T = d_0 d_1$, and $u_i = r_0^i P_i^*/K$. Then the first Lyapunov coefficient of system (1) at the positive equilibrium E_i, is

$$l_1^i = \frac{\omega_i b_4^i d_2^4 + b_3^i d_2^3 + b_2^i d_2^2 + b_1^i d_2 + \omega_i b_0^i}{(P_i^*)^2 \prod_{k=0}^2 (d_k^2 + \omega_i^2)\left[(L_5^i L_4^i - L_6^i L_3^i)^2 + (L_5^i L_4^i + L_6^i L_3^i)^2\right]},$$

where

$$L_1^i = d_0 d_1 d_2 - 4\omega_i^2(d_0 + d_1 + d_2), \quad L_2^i = 2\omega_i(d_0 d_1 + d_0 d_2 + d_1 d_2 - 4\omega_i^2),$$

$$L_3^i = \frac{r_0^i P_i^*}{K} L_1^i - 2\omega_i L_2^i + \delta P_i^* m\beta_1\beta_2, \quad L_4^i = \frac{r_0^i P_i^*}{K} L_2^i - 2\omega_i L_1^i,$$

$$L_5^i = 1 + \frac{r_0^i P_i^*}{K}\sum_{k=0}^2 \frac{d_k}{d_k^2 + \omega_i^2} + \omega_i^2 \sum_{s=0}^2 \frac{1}{d_s^2 + \omega_i^2}, \quad L_6^i = \omega_i\left(\sum_{k=0}^2 \frac{d_k}{d_k^2 + \omega_i^2} - \frac{r_0^i P_i^*}{K}\sum_{s=0}^2 \frac{1}{d_s^2 + \omega_i^2}\right),$$

and

$$\begin{aligned} b_0^i = {} & 4\omega_i^2(4S^2\omega_i^2 + T^2 - 8T^2\omega_i^2 + 16\omega_i^4)\left[u_i^3(T^2 + (2S^2 - 4T)\omega_i^2 + 3\omega_i^4) + u_i\omega_i^4(S^2 - 2T + 2\omega_i^2)\right. \\ & - 2S\omega_i^2(u_i^2 + \omega_i^2)(T + \omega_i^2) - 2P_i^*\delta m\beta_1\beta_2\omega_i^2\left[4Su_i^2(T^2 + (2S^2 - 4T)\omega_i^2 + 3\omega_i^4) + 3u_i(T^3\right. \\ & - 8T^2\omega_i^2 + (19T - 10S^2)\omega_i^4 - 12\omega_i^6) - S\omega_i^2\left(7T^2 - (21T - 6S^2)\omega_i^2 - 4\omega_i^4\right)\left.\right] \\ & - (P_i^*\delta m\beta_1\beta_2)^2\left[u_i(T^2 + (2S^2 - 4T)\omega_i^2 + 3\omega_i^4) + S\omega_i^2(T + \omega_i^2)\right], \end{aligned}$$

$$
\begin{aligned}
b_1^i = & -\omega_i^2\Big(8\omega_i^2(u_i^2+\omega_i^2)(S^2\omega_i^2+T^2-2T^2\omega_i^2+\omega_i^4)(4S^2\omega_i^2+T^2-8T\omega_i^2+16\omega_i^4)-(P_i^*\delta m\beta_1\beta_2)\\
&\big[2u_i^2(2S^2T\omega_i^2-8S^2\omega_i^4+T^3-8T^2\omega_i^2+19T\omega_i^4-12\omega_i^6)+3Su_i\omega_i^2(T+\omega_i^2)(T+2\omega_i^2)\\
&+\omega_i^2(4T^3+T(9S^2-22T)\omega_i^2+2(13T-3S^2)\omega_i^4-8\omega_i^6)\big]\\
&-(P_i^*\delta m\beta_1\beta_2)^2(S^2\omega_i^2+T^25-2T\omega_i^2+\omega_i^4)\Big),
\end{aligned}
$$

$$
\begin{aligned}
b_2^i = & \omega_i^2\Big((4S^2\omega_i^2+T^2-8T\omega_i^2+16\omega_i^4)\big[u_i^3(T^2+6(S^2-2T)\omega_i^2+11\omega_i^4)-u_i\omega_i^2(4T^2-(S^2-2T)\omega_i^2\\
&-6\omega_i^4)-10S\omega_i^2(u_i^2+\omega_i^2)(T+\omega_i^2)\big]-(P_i^*\delta m\beta_1\beta_2)\big[8Su_i^2\omega_i^2(S^2-2T+2\omega_i^2)+3u_i(T^3\\
&-T(S^2+10T)\omega_i^2-(16S^2-29T)\omega_i^4-20\omega_i^6)-2S\omega_i^2(8T^2+(7S^2-23T)\omega_i^2-3\omega_i^4)\big]\\
&+(P_i^*\delta m\beta_1\beta_2)^2\big[u_i(S^2-2T+2\omega_i^2)-S(T+\omega_i^2)\big]\Big),
\end{aligned}
$$

$$
\begin{aligned}
b_3^i = & -\omega_i^2\Big(2(u_i^2+\omega_i^2)(S^2\omega_i^2+T^2-2T\omega_i^2+\omega_i^4)(4S^2\omega_i^2+T^2-8T\omega_i^2+16\omega_i^4)-(P_i^*\delta m\beta_1\beta_2)\\
&\big[2u_i^2(S^2T-4S^2\omega_i^2-2T\omega_i^2+\omega_i^4)(4S^2\omega_i^2+T^2-8T\omega_i^2+16\omega_i^4)\big]-(P_i^*\delta m\beta_1\beta_2)^2\\
&\big[2u_i^2(S^2T-4S^2\omega_i^2-2T^2+10T\omega_i^2-8\omega_i^4)-3Su_i(2S^2\omega_i^2+T^2-7T\omega_i^2)-T^3\\
&+4T(S^2+2T)\omega_i^2+(14S^2-19T)\omega_i^4+12\omega_i^6\big]\Big),
\end{aligned}
$$

$$
b_4^i = (4S^2\omega_i^2+T^2-8T\omega_i^2+16\omega_i^4)\big[u_i^3(S^2-2T+2\omega_i^2)-2S(u_i^2+\omega_i^2)(T+\omega_i^2)+u_i(\omega_i^4-T^2)\big].
$$

Theorem 3.7 When $r=r_0^i$ and $l_1^i\neq 0$, system (1) undergoes a nondegenerate Hopf bifurcation near E_i. Moreover, if $l_1^i<0$, a supercritical Hopf bifurcation occurs, and the bifurcating periodic solution is stable; if $l_1^i>0$, a subcritical Hopf bifurcation occurs, and the bifurcating periodic solution is unstable.

Proof By **Theorem 3.6**, at $r=r_0^i$, the linearization of system (1) at E_i has a pair of simple purely imaginary eigenvalues $\pm\mathrm{i}\omega$, while all other eigenvalues have negative real parts. Therefore, the center manifold is two dimensional, and in suitable complex coordinates the normal form on the center manifold is

$$
z' = (\xi_i(r)+\mathrm{i}\omega_i(r))\,z + c_1^i z|z|^2 + O\left(|z|^4+|r-r_0^i||z|^2\right),
$$

where $\xi_i(r)=\operatorname{Re}\lambda_i(r)$ and $\xi_i(r_0^i)=0$.

Let $z=\rho e^{\mathrm{i}\theta}$, with $\rho\geq 0$. Substitution into the normal form, followed by separation of the real and imaginary parts, gives

$$
\rho' = \rho\left[\xi_i(r)+l_1^i\rho^2+O\left(\rho^4+|r-r_0^i|\rho^2\right)\right].
$$

To obtain the positive solution of the above equation, let $\rho'=0$, we have

$$
\xi_i(r)+l_1^i\rho^2+O\left(\rho^4+|r-r_0^i|\rho^2\right)=0.
$$

When $l_1^i\neq 0$, the implicit function theorem gives

$$
\rho^2(r) = -\frac{\xi_i(r)}{l_1^i}+o(|\xi_i(r)|) = -\frac{\xi_i'(r_0^i)}{l_1^i}(r-r_0^i)+o(|r-r_0^i|).
$$

Thus the leading order condition for the existence of small amplitude periodic solutions is

$$
-\frac{\xi_i'(r_0^i)}{l_1^i}(r-r_0^i)>0.
$$

Finally, to determine stability, denote the right hand side of the radial equation by $G_i(\rho, r)$. At a nonzero small amplitude equilibrium,

$$\frac{\partial G_i}{\partial \rho} = 2l_1^i \rho^2 + o(\rho^2).$$

Therefore, if $l_1^i < 0$, the radial derivative is negative and the bifurcating periodic orbit is asymptotically stable; if $l_1^i > 0$, the radial derivative is positive and the bifurcating periodic orbit is unstable.

To characterize the bifurcation arising when the first Lyapunov coefficient satisfies $l_1^i = 0$, let l_2^i be the second Lyapunov coefficient of system (1) at E_i. We first clarify the state variables and the spaces used in the calculation. Recall that, after translating the equilibrium E_i to the origin, the state variable is

$$Z = (u, v, x, y)^T = (P - P_i^*,\, Q - Q_i^*,\, X - X_i^*,\, B - B_i^*)^T \in \mathbb{R}^4.$$

Thus, Z is the four-dimensional real state variable of the translated system, and $Z = 0$ corresponds to E_i. In particular, the original system and its local center manifold are defined in the real phase space $\mathbb{R}^4$.

At the Hopf point, the real matrix M_i has the simple eigenvalues $\pm \mathrm{i}\omega_i$. The corresponding eigenvectors are generally not real. Hence, only for the purpose of the eigenvector and normal-form calculations, we use the complexification of the real phase space, $\mathbb{R}^4 \subset \mathbb{C}^4$. Let $q_i \in \mathbb{C}^4$ satisfy

$$M_i q_i = \mathrm{i}\omega_i q_i.$$

Since M_i is real,

$$M_i \bar{q}_i = -\mathrm{i}\omega_i \bar{q}_i.$$

The use of $\mathbb{C}^4$ here does not change the state space of the original system; it only provides a convenient representation of the two real center directions associated with the conjugate eigenvalue pair.

More precisely, if $z \in \mathbb{C}$, then

$$z q_i + \bar{z}\, \bar{q}_i = 2\,\mathrm{Re}(z q_i) \in \mathbb{R}^4.$$

Conversely, the two-dimensional real center subspace generated by $\mathrm{Re}\, q_i$ and $\mathrm{Im}\, q_i$ can be represented in this form. Therefore, the single complex number z is used to encode the two real center coordinates through its real and imaginary parts. Thus, z is not an additional state variable of system (1); it is a complex coordinate used to describe the center component of the real state Z. The coefficient of $\bar{q}_i$ must be $\bar{z}$ so that the resulting vector remains in $\mathbb{R}^4$.

The adjoint eigenvector introduced above is normalized by $p_i = \frac{\widetilde{p}_i}{\Psi_i}$, $\langle p_i, q_i \rangle = 1$. For real vectors $U = (U_1, U_2, U_3, U_4)^T \in \mathbb{R}^4$ and $V = (V_1, V_2, V_3, V_4)^T \in \mathbb{R}^4$, the symmetric bilinear map associated with the quadratic part is

$$B_i(U, V) = \left(-\frac{2r_0^i}{K} U_1 V_1 - \delta(U_1 V_4 + U_4 V_1), 0, 0, 0 \right)^T.$$

Because the center-manifold calculation involves the complex vectors q_i, $\bar{q}_i$, and the complex coefficient vectors introduced below, the same formula is extended complex bilinearly from $\mathbb{R}^4 \times \mathbb{R}^4$ to $\mathbb{C}^4 \times \mathbb{C}^4$. Accordingly, expressions such as $B_i(q_i, q_i)$ and $B_i(q_i, \bar{q}_i)$ are understood in this complexified sense.

The local center manifold through $Z = 0$ is a two-dimensional real manifold contained in $\mathbb{R}^4$ and tangent at the origin to the real center subspace described above. Using the complex coordinate z for these two real center directions, we write its local parameterization as

$$Z = H_i(z, \bar{z}).$$

Since the center manifold is tangent to the center subspace at $Z = 0$, the linear part of H_i is $zq_i + \bar{z}\,\bar{q}_i$. To determine the fifth-order normal-form coefficient, we expand

$$H_i(z, \bar{z}) = zq_i + \bar{z}\,\bar{q}_i + \sum_{2 \le j+k \le 5} \frac{1}{j!k!} \chi^i_{jk} z^j \bar{z}^{\,k} + O(|z|^6), \tag{5}$$

where j, k are nonnegative integers and $\chi^i_{jk} \in \mathbb{C}^4$. Although the individual coefficient vectors χ^i_{jk} may be complex, the parameterization must represent a real state $Z \in \mathbb{R}^4$. Therefore, $\chi^i_{kj} = \overline{\chi^i_{jk}}$, which ensures that the terms in the expansion occur in conjugate pairs and hence that $H_i(z, \bar{z}) \in \mathbb{R}^4$ whenever $z = \overline{z}$.

We next consider the dynamics of the complex center coordinate z. For a monomial $z^j \bar{z}^{\,k}$ in the z-equation, resonance with the eigenvalue $\mathrm{i}\omega_i$ occurs when $(j-k)\mathrm{i}\omega_i = \mathrm{i}\omega_i$, that is, when $j - k = 1$.

After eliminating the nonresonant terms by a near-identity transformation, the resonant terms up to fifth order are therefore $z^2\bar{z}$ and $z^3\bar{z}^{\,2}$. The reduced equation on the center manifold takes the form

$$z' = \mathrm{i}\omega_i z + \frac{1}{2}\gamma^i_{21} z^2 \bar{z} + \frac{1}{12}\gamma^i_{32} z^3 \bar{z}^{\,2} + O(|z|^6),$$

where $\gamma^i_{21}, \gamma^i_{32} \in \mathbb{C}$. set $z = \rho e^{\mathrm{i}\theta}$, we have,

$$\rho' = \frac{1}{2}\,\mathrm{Re}(\gamma^i_{21})\rho^3 + \frac{1}{12}\,\mathrm{Re}(\gamma^i_{32})\rho^5 + O(\rho^6).$$

Therefore

$$l^i_2 = \frac{1}{12}\,\mathrm{Re}\,\gamma^i_{32}.$$

The derivation of the explicit expression for γ^i_{32} is presented below[40]. Substituting these expansions of Eq.(5) into the center-manifold invariance equation

$$\frac{\partial H_i}{\partial z} z' + \frac{\partial H_i}{\partial \bar{z}} \bar{z}' = M_i H_i + \frac{1}{2} B_i(H_i, H_i)$$

and equating the coefficients of $z^j \bar{z}^{\,k}$ yield the required homological equations. Since $\pm\mathrm{i}\omega_i$ are simple and all the remaining eigenvalues of M_i have negative real parts, M_i, $2\mathrm{i}\omega_i I - M_i$, and $3\mathrm{i}\omega_i I - M_i$ are invertible.

At second order,

$$\chi_{20}^i = (2\mathrm{i}\omega_i I - M_i)^{-1} B_i(q_i, q_i), \chi_{11}^i = -M_i^{-1} B_i(q_i, \bar{q}_i),$$

where I is the identity matrix. At third order,

$$\gamma_{21}^i = \left\langle p_i, B_i(\bar{q}_i, \chi_{20}^i) + 2B_i(q_i, \chi_{11}^i) \right\rangle, \chi_{30}^i = (3\mathrm{i}\omega_i I - M_i)^{-1} \left[3B_i(q_i, \chi_{20}^i) \right].$$

The resonant coefficient χ_{21}^i is determined by

$$(\mathrm{i}\omega_i I - M_i)\chi_{21}^i = B_i(\bar{q}_i, \chi_{20}^i) + 2B_i(q_i, \chi_{11}^i) - \gamma_{21}^i q_i, \langle p_i, \chi_{21}^i \rangle = 0.$$

By the definition of γ_{21}^i, the right-hand side is orthogonal to p_i; hence the Fredholm solvability condition is satisfied, the normalization $\langle p_i, \chi_{21}^i \rangle = 0$ makes the solution unique.

Because $l_1^i = 0$, we have $\mathrm{Re}\,\gamma_{21}^i = 0, \gamma_{21}^i + \overline{\gamma_{21}^i} = 0$. The fourth-order coefficients required at fifth order are therefore

$$\chi_{31}^i = (2\mathrm{i}\omega_i I - M_i)^{-1} \Big[3B_i(\chi_{20}^i, \chi_{11}^i) + B_i(\bar{q}_i, \chi_{30}^i) + 3B_i(q_i, \chi_{21}^i) - 3\gamma_{21}^i \chi_{20}^i \Big],$$
$$\chi_{22}^i = -M_i^{-1} \Big[2B_i(\chi_{11}^i, \chi_{11}^i) + 2B_i(q_i, \overline{\chi_{21}^i}) + 2B_i(\bar{q}_i, \chi_{21}^i) + B_i(\overline{\chi_{20}^i}, \chi_{20}^i) \Big].$$

In the general fourth-order equation for χ_{22}^i, there is also a term $-2(\gamma_{21}^i + \overline{\gamma_{21}^i})\chi_{11}^i$, which vanishes here because $l_1^i = 0$. At fifth order, let R_{32}^i denote the vector inside the inner product in the formula below. The complete homological equation for the resonant monomial $z^3 \bar{z}^2$ is

$$(\mathrm{i}\omega_i I - M_i)\chi_{32}^i = R_{32}^i - \gamma_{32}^i q_i - \big(6\gamma_{21}^i + 3\overline{\gamma_{21}^i}\big)\chi_{21}^i.$$

Taking the inner product with p_i and using $\langle p_i, \chi_{21}^i \rangle = 0$, the Fredholm solvability condition gives

$$\gamma_{32}^i = \Big\langle p_i, 2B_i(\bar{q}_i, \chi_{31}^i) + 3B_i(q_i, \chi_{22}^i) + B_i(\overline{\chi_{20}^i}, \chi_{30}^i) + 3B_i(\overline{\chi_{21}^i}, \chi_{20}^i) + 6B_i(\chi_{11}^i, \chi_{21}^i) \Big\rangle.$$

Consequently,

$$l_2^i = \frac{1}{12}\,\mathrm{Re}\Big\langle p_i, 2B_i(\bar{q}_i, \chi_{31}^i) + 3B_i(q_i, \chi_{22}^i) + B_i(\overline{\chi_{20}^i}, \chi_{30}^i) + 3B_i(\overline{\chi_{21}^i}, \chi_{20}^i) + 6B_i(\chi_{11}^i, \chi_{21}^i) \Big\rangle.$$

We then have the following result.

Theorem 3.8 Suppose that d_2 is an additional bifurcation parameter.If $b_4^i b_0^i < 0$,there exists $d_2 = d_2^i$ such that $l_1^i = 0$ and $l_2^i \neq 0$, then system (1) undergoes Bautin bifurcation at (r_0^i, d_2^i).

Proof Since the denominator of l_1^i is strictly positive, $l_1^i = 0$ if and only if its numerator vanishes. In the polynomial representation above, define

$$\mathcal{P}_i(d_2) = \omega_i b_4^i d_2^4 + b_3^i d_2^3 + b_2^i d_2^2 + b_1^i d_2 + \omega_i b_0^i.$$

For fixed i, $\mathcal{P}_i$ is continuous on $[0, +\infty)$. Moreover,

$$\mathcal{P}_i(0) = \omega_i b_0^i, \quad \lim_{d_2 \to +\infty} \frac{\mathcal{P}_i(d_2)}{d_2^4} = \omega_i b_4^i.$$

When $b_4^i b_0^i < 0$, the two quantities $\omega_i b_0^i$ and $\omega_i b_4^i$ have opposite signs. Hence there exists a sufficiently large value $\mathcal{M} > 0$ of the parameter d_2 such that

$$\mathcal{P}_i(0)\mathcal{P}_i(\mathcal{M}) < 0.$$

By the intermediate value theorem, there exists $d_2^i \in (0, \mathcal{M})$ such that $l_1(d_2^i) = 0$.

By $l_2^i \neq 0$, consider a point (r_0, d_2) in a sufficiently small neighborhood of the critical parameter point (r_0^i, d_2^i),introduce $\alpha_1 = \xi_i(r_0, d_2)$ and $\alpha_2 = l_1^i(r_0, d_2)$ as local bifurcation parameter. Then the radial normal form is

$$\rho' = \rho\left[\alpha_1 + \alpha_2\rho^2 + l_2^i\rho^4 + O(\rho^6)\right] := \rho\varphi(\rho),$$

where

$$\varphi(\rho) = \alpha_1 + \alpha_2\rho^2 + l_2^i\rho^4 + O(\rho^6).$$

First, $\rho = 0$ corresponds to the equilibrium E_i. By **Theorem 3.6**, when $\alpha_1 = \xi_i(r_0, d_2) = 0$, the critical pair of eigenvalues crosses the imaginary axis transversely, and hence a Hopf bifurcation occurs. Nonzero periodic solutions correspond to positive equilibria of the radial equation. Let $y = \rho^2$. Ignoring higher order terms, the nonzero periodic solutions satisfy

$$\alpha_1 + \alpha_2 y + l_2^i y^2 = 0.$$

Thus the necessary condition for nonzero periodic solutions is

$$\alpha_2^2 - 4l_2^i\alpha_1 \geq 0.$$

When $\alpha_2^2 - 4l_2^i\alpha_1 = 0$, the two nonzero periodic solutions coincide. At this point the radial equation has a multiple root, corresponding to collision and disappearance of a stable periodic solution and an unstable periodic solution, namely a saddle node bifurcation of limit cycles.

We further discuss the stability of periodic solutions. A nonzero periodic solution corresponds to a positive equilibrium $\rho^* > 0$ of the radial equation and hence satisfies $\varphi(\rho^*) = 0$. Therefore, the derivative of the radial equation at ρ^* is

$$\frac{\mathrm{d}}{\mathrm{d}\rho}\big(\rho\varphi(\rho)\big)\Big|_{\rho=\rho^*} = \rho^*\varphi'(\rho^*) = 2(\rho^*)^2\left(\alpha_2 + 2l_2^i(\rho^*)^2\right) + O((\rho^*)^6).$$

Let $y = (\rho^*)^2$. For the truncated radial equation, the roots $y_\pm$ satisfy

$$\alpha_2 + 2l_2^i y_\pm = \pm\sqrt{\alpha_2^2 - 4l_2^i\alpha_1}.$$

Therefore, in the region where two periodic solutions coexist, one branch is stable and the other is unstable. The branch with negative radial derivative corresponds to the stable periodic solution, while the branch with positive radial derivative corresponds to the unstable periodic solution. The two branches coincide and fold on the curve. Hence (r_0^i, d_2^i) is a Bautin bifurcation point.

According to the Bautin bifurcation criterion in Section 2 of reference[26], we now discuss the number of small amplitude limit cycles near the positive equilibrium of system (1) when Bautin bifurcation occurs. For convenience, let $D_i = \alpha_2^2 - 4l_2^i\alpha_1$.

Theorem 3.9 Suppose that system (1) undergoes a Bautin bifurcation near the positive equilibrium E_i. The number of limit cycles satisfies: (1) If $D_i < 0$, then no limit cycle exists near E_i; (2) If $D_i > 0$, then one or two small amplitude limit cycles exist near E_i; (3) And if $D_i = 0$, then one multiple limit cycle exists near E_i.

Proof (1) If $D_i < 0$, the Eq. has no real roots; hence no small amplitude limit cycle exists.

(2) If $D_i > 0$, the number of small amplitude limit cycles near E_i is equal to the number of positive roots of

$$\alpha_1 + \alpha_2 y + l_2^i y^2 = 0.$$

The roots are

$$y_\pm = \frac{-\alpha_2 \pm \sqrt{D_i}}{2l_2^i}.$$

By Vieta's formula,we have

$$y_+ y_- = \frac{\alpha_1}{l_2^i}, y_+ + y_- = -\frac{\alpha_2}{l_2^i}.$$

If $\alpha_1 l_2^i < 0$, there is exactly one positive root, corresponding to one small amplitude limit cycle. If $\alpha_1 l_2^i > 0$ and $\alpha_2 l_2^i < 0$, the two roots have the same sign and a positive sum, so both roots are positive and two limit cycles exist. If $\alpha_1 l_2^i > 0$ and $\alpha_2 l_2^i > 0$, the two roots have the same sign and a negative sum, so both roots are negative and no limit cycle exists.

(3) If $D_i = 0$, the Eq. has the multiple root $y_* = -\alpha_2/(2l_2^i)$. If $\alpha_2 l_2^i < 0$, then $y_* > 0$, and one multiple limit cycle exists.

In summary, near the Bautin critical point (r_0^i, d_2^i) , if $D_i < 0$, no small amplitude limit cycle exists near E_i; if $D_i = 0$, one multiple limit cycle exists near E_i. If $D_i > 0$ and $\alpha_1 l_2^i > 0$, $\alpha_2 l_2^i > 0$, no limit cycle exists near E_i; if $D_i > 0$ and $\alpha_1 l_2^i < 0$, one small amplitude limit cycle exists near E_i; if $D_i > 0$ and $\alpha_1 l_2^i > 0$, $\alpha_2 l_2^i < 0$, two limit cycles exist near E_i.

4 Stability Analysis of Pseudo Equilibria

4.1 Switching surface and sliding region

Let the switching function be $\Phi(P, Q, X, B) = P - P_a$. The switching surface of system (1) is

$$\Sigma = \{(P, Q, X, B) \in \mathbb{R}_+^4 \mid \Phi = 0\}.$$

On the two sides of the switching surface, the system is described by different smooth vector fields:

$$F^- = \begin{pmatrix} rP(1-P/K) - \delta BP \\ mP - d_0 Q \\ \beta_1 Q - d_1 X \\ \alpha + \beta_2 X - d_2 B \end{pmatrix}, \quad F^+ = \begin{pmatrix} rP(1-P/K) + \eta P - \delta BP \\ mP - d_0 Q \\ \beta_1 Q - d_1 X \\ \alpha + \beta_2 X - d_2 B \end{pmatrix}.$$

To illustrate the sliding region and the crossing region, take the normal vector of Σ as $\nabla H = (1, 0, 0, 0)$. The Lie derivatives of the two subsystems on Σ are

$$L_{F^-}(H) = \langle \nabla H, F^- \rangle = rP_a \left(1 - \frac{P_a}{K}\right) - \delta B P_a,$$
$$L_{F^+}(H) = \langle \nabla H, F^+ \rangle = rP_a \left(1 - \frac{P_a}{K}\right) + \eta P_a - \delta B P_a.$$

Define $\sigma(P_a, Q, X, B) = L_{F^-}(H) \cdot L_{F^+}(H)$. According to the sign of σ, Σ can be divided into the following disjoint regions:

(1) **Crossing region** Σ_c: $\sigma > 0$. Trajectories cross the switching surface transversally.

(2) **Sliding region** Σ_s: $\sigma < 0$. The two vector fields point toward or away from each other across the switching surface.

Furthermore, the sliding region Σ_s can be subdivided as follows:

(1) **Attracting sliding region** Σ_a: $L_{F^-}(H) > 0$ and $L_{F^+}(H) < 0$; Trajectories approach the switching surface from both sides.

(2) **Repelling sliding region** Σ_r: $L_{F^-}(H) < 0$ and $L_{F^+}(H) > 0$; Trajectories move away from the switching surface on both sides.

Note that system (1) has only a repelling sliding region Σ_r, with explicit expression

$$\Sigma_r = \left\{ (P_a, Q, X, B) \in \Sigma \;\middle|\; \frac{r(K - P_a)}{\delta K} < B < \frac{r(K - P_a)}{\delta K} + \frac{\eta}{\delta} \right\}.$$

4.2 Existence and stability of pseudo equilibria

In the interior of the repelling sliding region Σ_r, the dynamics of the system are described by the sliding vector field defined by Filippov's convex method:

$$F_s = \lambda F^+ + (1 - \lambda) F^-,$$

where $\lambda \in [0, 1]$ is determined by the normal component balance condition

$$\lambda L_{F^+}(H) + (1 - \lambda) L_{F^-}(H) = 0.$$

Also,

$$\lambda = \frac{L_{F^-}(H)}{L_{F^-}(H) - L_{F^+}(H)} = \frac{\delta}{\eta} B - \frac{r}{\eta} \left(1 - \frac{P_a}{K}\right).$$

Thus the tangential sliding equation is

$$\begin{cases} \dfrac{\mathrm{d}Q}{\mathrm{d}t} = mP - d_0 Q, \\ \dfrac{\mathrm{d}X}{\mathrm{d}t} = \beta_1 Q - d_1 X, \\ \dfrac{\mathrm{d}B}{\mathrm{d}t} = \alpha + \beta_2 X - d_2 B. \end{cases} \tag{6}$$

If a point $E_p = (P_a, Q^*, X^*, B^*) \in \Sigma_r$ makes all right hand sides of the sliding system equal to zero, then E_p is called a pseudo equilibrium of the Filippov system. Setting the right hand side of system (6) equal to zero gives

$$E_p = \left(P_a, \frac{mP_a}{d_0}, \frac{\beta_1 m P_a}{d_0 d_1}, \frac{\alpha}{d_2} + \frac{\beta_1 \beta_2 m P_a}{d_0 d_1 d_2} \right).$$

Theorem 4.1 The pseudo equilibrium E_p is exponentially asymptotically stable in Σ_r.

Proof The eigenvalues of the Jacobian matrix at the pseudo equilibrium are

$$\lambda_1 = -d_0 < 0, \quad \lambda_2 = -d_1 < 0, \quad \lambda_3 = -d_2 < 0.$$

Therefore, E_p is locally asymptotically stable on Σ_r. Next we prove exponential asymptotic stability. Let

$$u = Q - Q^*, \quad v = X - X^*, \quad w = B - B^*.$$

Then the sliding system (6) can be written as

$$Z' = MZ,$$

where

$$Z = (u, v, w)^T \in \mathbb{R}^3_+, G = \begin{pmatrix} -d_0 & 0 & 0 \\ \beta_1 & -d_1 & 0 \\ 0 & \beta_2 & -d_2 \end{pmatrix}.$$

Since M is a lower triangular matrix and all of its eigenvalues are negative, by the Lyapunov equation theorem there exists a positive definite matrix

$$N = \begin{pmatrix} n_{11} & n_{12} & \dfrac{\beta_1 \beta_2}{2d_2(d_0+d_2)(d_1+d_2)} \\ n_{12} & \dfrac{d_2(d_1+d_2)+\beta_2^2}{2d_1 d_2 (d_1+d_2)} & \dfrac{\beta_2}{2d_2(d_1+d_2)} \\ \dfrac{\beta_1\beta_2}{2d_2(d_0+d_2)(d_1+d_2)} & \dfrac{\beta_2}{2d_2(d_1+d_2)} & \dfrac{1}{2d_2} \end{pmatrix},$$

where

$$n_{11} = \frac{d_1 d_2 (d_0+d_1)(d_0+d_2)(d_1+d_2) + \beta_1^2 \left[d_2(d_0+d_2)(d_1+d_2) + \beta_2^2 (d_0+d_1+d_2) \right]}{2d_0 d_1 d_2 (d_0+d_1)(d_0+d_2)(d_1+d_2)},$$

$$n_{12} = \frac{\beta_1 \left[d_2(d_0+d_2)(d_1+d_2) + \beta_2^2 (d_0+d_1+d_2) \right]}{2d_1 d_2 (d_0+d_1)(d_0+d_2)(d_1+d_2)}.$$

It satisfies

$$G^T N + NG = -I.$$

Taking $V(Z) = Z^T NZ$ and differentiating gives

$$V' = Z^T(G^T N + NG)Z = - \|Z\|^2 < 0, \quad Z \neq 0.$$

Therefore, the origin $Z = 0$ is an exponentially asymptotically stable equilibrium of the error system. Hence

$$\lim_{t\to\infty} Q(t) = Q^*, \quad \lim_{t\to\infty} X(t) = X^*, \quad \lim_{t\to\infty} B(t) = B^*.$$

Thus the pseudo equilibrium E_p is exponentially asymptotically stable in Σ_r.

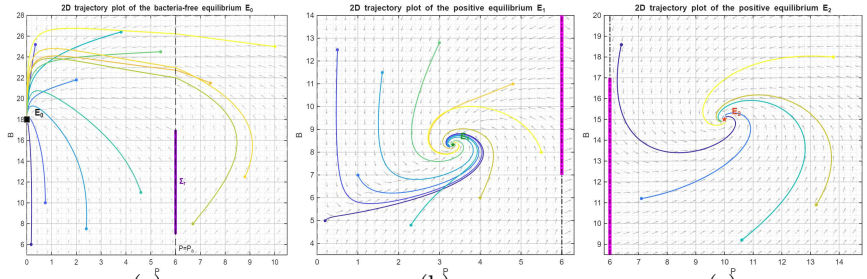
5 Numerical Simulations

This section verifies the theoretical results obtained above through numerical simulations. The numerical simulations mainly include four aspects: stability of the bacteria free equilibrium and positive equilibria, stability of the pseudo equilibrium on the switching surface, periodic oscillations induced by Hopf bifurcation, and changes in the number of small amplitude limit cycles near a Bautin bifurcation.

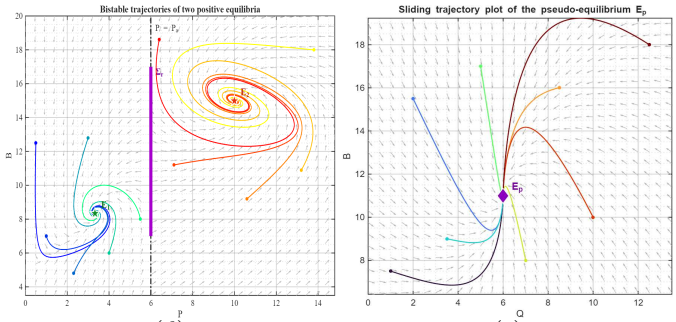
First, consider the stability of system (1) equilibria. Take

$$r = m = d_0 = \beta_1 = d_1 = \beta_2 = d_2 = \eta = 1, \quad K = 20, \quad \delta = 0.1, \quad P_a = 6.$$

When $\alpha = 18$, $R_{01} = 0.56 < 1$. According to **Theorem 3.2**, system (1) has a stable bacteria free equilibrium E_0. When $\alpha = 5$, $R_{01} = 2 > 1$, $R_{02} = 4 > 1$, $s_1 = 9.4 > 0$, and $s_2 = 14.8 > 0$. By **Theorem 3.2**, the system (1) has a stable low bacterial load positive equilibrium E_1 on the low bacterial load branch and a stable high bacterial load positive equilibrium E_2 on the high bacterial load branch. **Corollary 3.1** also implies that the system (1) exhibits bistability in this parameter region. Furthermore, on the switching surface there exists a pseudo equilibrium E_p. Since this point satisfies the existence and stability conditions in the sliding region, E_p is a pseudo equilibrium of the system (6) and is exponentially asymptotically stable in the sliding region.



(a) (b) (c)



(d) (e)

Figure 2: Trajectory diagrams of equilibria. (a) Two dimensional trajectory diagram of the bacteria-free equilibrium E_0; (b) Two dimensional phase diagram of the equilibrium E_1; (c) Two dimensional trajectory diagram of the equilibrium E_2; (d) trajectory diagram showing bistability of positive equilibria; (e) sliding trajectory diagram of the pseudo equilibrium E_p. Colored curves denote trajectories, the purple line denotes the sliding region, gray arrows denote the vector field direction, and the black dashed line denotes the threshold.

Figure 2(a) shows that, regardless of whether the initial value of a trajectory lies in the low bacterial load domain or the high bacterial load domain, the system (1) eventually tends to the bacteria-free equilibrium E_0. Thus the bacteria-free equilibrium $E_0 = (0, 0, 0, 18)$ is locally asymptotically stable. Figures 2(b) and 2(c) give the phase diagrams on the low bacterial load branch and the high bacterial load branch, respectively. In the corresponding basins of attraction, the trajectories converge to the positive equilibria $E_1 = (3.3, 3.3, 3.3, 8.3)$ and $E_2 = (10, 10, 10, 15)$, indicating that both positive equilibria are locally asymptotically stable. Figure 2(d) further shows that, under the same parameter set, different initial values may tend either to the low bacterial load equilibrium E_1 or to the high bacterial load equilibrium E_2, which indicates a bistable structure induced by the quorum sensing threshold. Figure 2(e) displays the sliding dynamics near the switching surface. Trajectories eventually converge to the pseudo equilibrium $E_p = (6, 6, 6, 11)$, showing that the pseudo equilibrium is exponentially asymptotically stable in the sliding region.

Second, numerical simulations are performed for the Hopf bifurcation near positive equilibria, and the first Lyapunov coefficient is used to determine the type of Hopf bifurcation. For the low bacterial load positive equilibrium E_1, take

$$r = 1.37,\ K = 100,\ \delta = 0.01,\ m = 0.5,\ d_0 = 0.1,$$
$$d_1 = 0.1,\ \beta_2 = 0.1,\ d_2 = 0.16,\ \beta_1 = 0.2,\ \alpha = 0.1,\ \eta = 0.2.$$

Taking d_2 as the bifurcation parameter, the equilibrium is $E_1 = (18, 90, 180, 82)$. At the critical value, the Jacobian matrix corresponding to E_1 has a pair of purely imaginary eigenvalues $\lambda_{1,2} = \pm 0.14\mathrm{i}$ and $\lambda_{3,4} = -0.3 \pm 0.14\mathrm{i}$, while the real parts of the remaining eigenvalues are negative. Hence the system (1) satisfies the critical conditions for Hopf bifurcation near E_1. Further computation

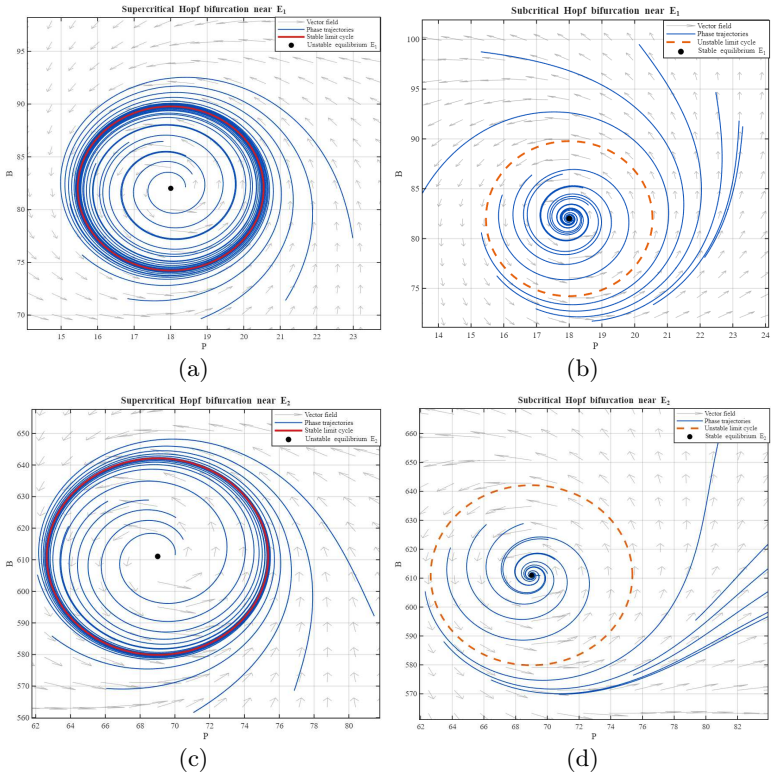
of the first Lyapunov coefficient at E_1 gives $l_1^1 = -1 < 0$. By **Theorem 3.7**, a supercritical Hopf bifurcation occurs near E_1, and the bifurcating periodic solution is stable.

For the high bacterial load branch E_2, take

$$r = 0.8,\ K = 803,\ \delta = 0.002,\ m = 0.45,\ d_0 = 0.08,$$
$$\beta_1 = 1,\ d_1 = 0.01,\ d_2 = 0.8,\ \beta_2 = 0.01,\ \alpha = 1.18,\ \eta = 0.35.$$

The high bacterial load positive equilibrium is $E_2 = (69, 391, 36390, 611)$. At E_2, the eigenvalues of the Jacobian matrix are $\lambda_{1,2} = 10^{-6} \pm 0.078\mathrm{i}$, $\lambda_3 = -0.16$, and $\lambda_4 = -0.8$. The real parts of $\lambda_{1,2}$ are approximately zero, and all other eigenvalues have negative real parts; thus the system (1) satisfies the critical conditions for Hopf bifurcation near E_2. Further computation of the first Lyapunov coefficient at E_2 gives $l_1^2 = -1 < 0$. By **Theorem 3.7**, a supercritical Hopf bifurcation occurs near E_2, and the bifurcating periodic solution is stable.

For comparison, the cases $l_1^1 > 0$ and $l_1^2 > 0$ are also simulated. By **Theorem 3.7**, they correspond to subcritical Hopf bifurcations near E_1 and E_2, respectively, and the bifurcating periodic solutions are unstable. The four corresponding local phase portraits are shown in Figure 3.



(a) (b)

(c) (d)

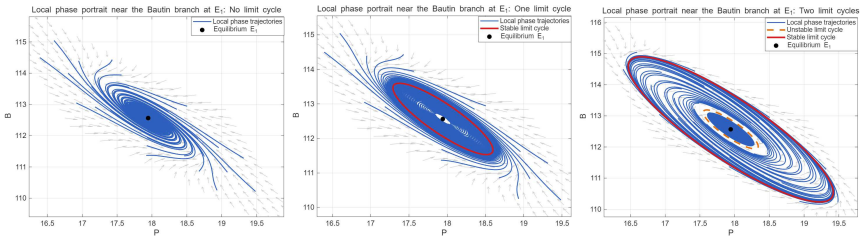
Figure 3: Local phase portraits of Hopf bifurcations near the positive equilibria. (a) Supercritical Hopf bifurcation near E_1; (b) subcritical Hopf bifurcation near E_1; (c) supercritical Hopf bifurcation near E_2; (d) subcritical Hopf bifurcation near E_2. Gray arrows denote the normalized vector field, blue curves denote phase trajectories, solid red curves denote stable limit cycles, dashed orange curves denote unstable limit cycles, and black dots denote equilibria.

Figures 3(a) and 3(c) illustrate the supercritical Hopf bifurcations near E_1 and E_2, respectively. In both cases, the equilibrium is unstable after the bifurcation, whereas trajectories initiated on either side of the periodic orbit approach the closed orbit. Hence the bifurcating limit cycle is stable. Figures 3(b) and 3(d) illustrate the corresponding subcritical configurations. Trajectories initiated inside the unstable periodic orbit spiral toward the stable equilibrium, while trajectories outside the periodic orbit move away from it. Therefore, the unstable limit cycle separates the local attraction region of the equilibrium from the outward-moving trajectories.

To further investigate the Bautin bifurcation in the degenerate Hopf case, assume that the first Lyapunov coefficient satisfies $l_1^i = 0$. According to Bautin bifurcation theory, the radius of a nonzero limit cycle is determined by an algebraic equation. Since $D = \alpha_1 + \alpha_2 y + l_{2i} y^2$, its discriminant determines whether limit cycles exist and how many there are, while the sign of the derivative of the radial equation at the corresponding radius determines the stability of the limit cycle. Select the following three groups of parameters:

$$(\alpha_1, \alpha_2, l_2^1) = (-0.02, -0.2, -1), \quad (0.02, -0.2, -1), \quad (-0.01, 0.4, -1).$$

The three parameter groups correspond to $D = -0.04 < 0$, $D = 0.12 > 0$, and $D = 0.12 > 0$, respectively. Near the low bacterial load positive equilibrium E_1, they correspond to three typical cases: no limit cycle, one small amplitude limit cycle, and two small amplitude limit cycles.



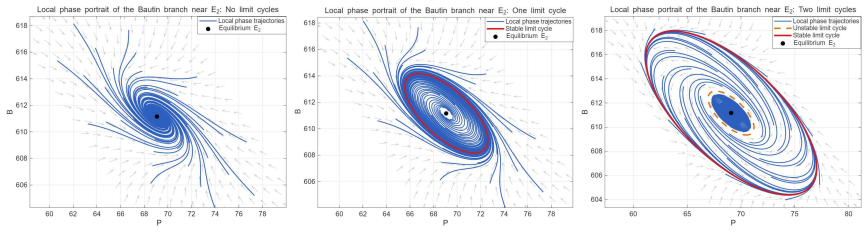
(a) (b) (c)

Figure 4: Phase portraits near the Bautin bifurcation at E_1: (a) no limit cycle; (b) one stable limit cycle; (c) two limit cycles, with the outer cycle stable and the inner cycle unstable. Blue curves denote trajectories, red curves denote stable limit cycles, and orange curves denote unstable limit cycles.

Figure 4 shows different dynamical behaviors caused by the Bautin bifurcation near the low bacterial load positive equilibrium E_1. In Figure 4(a),

trajectories eventually approach the neighborhood of the equilibrium and no closed orbit is observed, indicating that no small amplitude limit cycle exists in this parameter region. In Figure 4(b), the system (1) has one small amplitude closed orbit, and neighboring trajectories gradually approach it, indicating that this limit cycle is stable. In Figure 4(c), the system (1) has two small amplitude limit cycles simultaneously. The outer limit cycle attracts neighboring trajectories, whereas the inner limit cycle is repelling. Thus, this parameter region contains one stable limit cycle and one unstable limit cycle.

Using the same numerical strategy, simulations of the Bautin bifurcation near the high bacterial load positive equilibrium E_2 are carried out, and the results are shown in Figure 5.



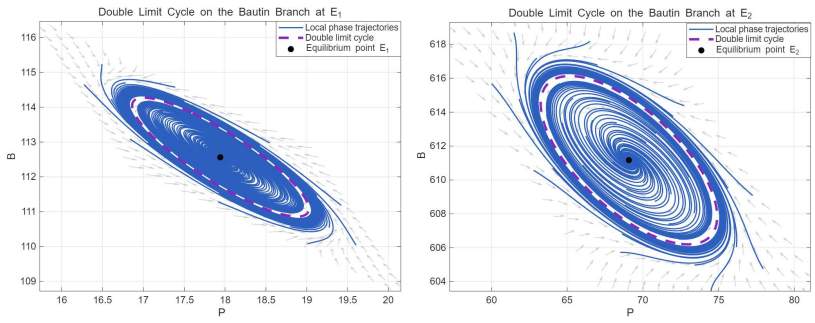
(a) (b) (c)

Figure 5: Phase portraits near the Bautin bifurcation at E_2: (a) no limit cycle; (b) one stable limit cycle; (c) two limit cycles, with the outer cycle stable and the inner cycle unstable. Blue curves denote trajectories, red curves denote stable limit cycles, and orange curves denote unstable limit cycles.

Figure 5 shows different dynamical behaviors caused by the Bautin bifurcation near the high bacterial load positive equilibrium E_2. Figure 5(a) corresponds to the case with no limit cycle; Figure 5(b) corresponds to the case with one stable small amplitude limit cycle; and Figure 5(c) corresponds to coexistence of two small amplitude limit cycles, where the outer limit cycle is stable and the inner limit cycle is unstable. This result indicates that Bautin bifurcation can occur not only on the low bacterial load branch but also on the high bacterial load branch, and the two branches have similar local dynamical structures.

Finally, consider the saddle node case of limit cycles in the Bautin bifurcation. By **Theorem 3.9**, when $D_i = 0$, the radial equation has a multiple root, and a stable limit cycle and an unstable limit cycle collide and merge into a multiple limit cycle. For the positive equilibria E_1 and E_2, take $\alpha_1 = -0.04$, $\alpha_2 = 0.4$, and $l_2^i = -1$. Then $D = 0$, and the equation has the multiple root $y = 0.2$.

Figure 6 gives numerical simulation results for the multiple limit cycles near E_1 and E_2, respectively. It can be seen that the closed orbit exhibits a semistable structure: trajectories approach the closed orbit from one side and move away from it on the other side. This indicates that a stable limit cycle and an unstable limit cycle collide on the saddle node bifurcation curve of limit cycles and merge



(a) (b)

Figure 6: Trajectory diagrams of multiple limit cycles in the Bautin bifurcation at positive equilibria. Panels (a)–(b) are phase diagrams of multiple limit cycles in the Bautin bifurcation at E_1 and E_2, respectively. The blue curve denotes the trajectory, and the purple curve denotes the multiple limit cycle formed.

into one multiple limit cycle.

In summary, the numerical simulations verify the theoretical analysis from the perspectives of equilibrium convergence, stability of sliding pseudo-equilibria, stable periodic solutions generated by Hopf bifurcation, multiple limit cycles induced by Bautin bifurcation, and formation of multiple limit cycles. The results show that the QS threshold can cause the interaction between pathogens and host immunity to induce complex system dynamics. As system parameters vary, the infection process may exhibit different states, such as bacterial clearance, low bacterial load chronic infection, high bacterial load persistent infection, or periodic immune oscillation. This shows that the quorum sensing threshold not only affects the stability of infection states but may also change the infection evolution process by inducing bifurcation, multistability, and limit cycle phenomena.

6 Sensitivity Analysis

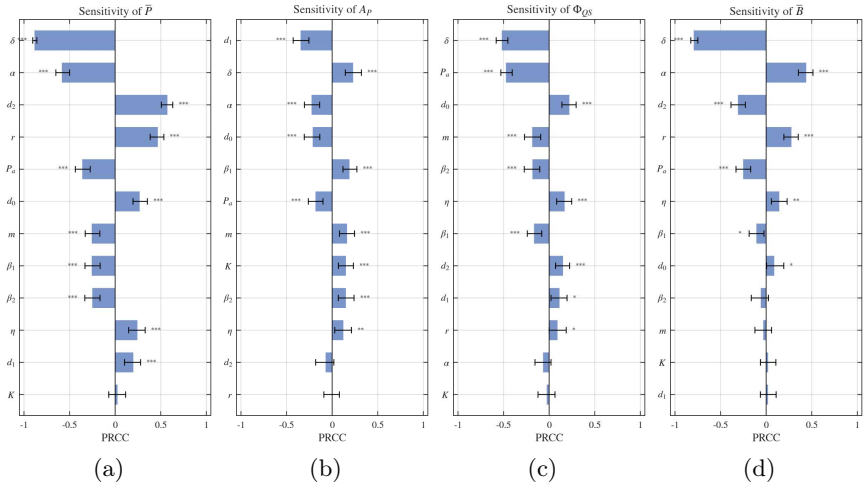
To further investigate the effects of model parameters on the long-term dynamical behavior of the system (1), this section performs global sensitivity analysis. Because the system (1) contains a discontinuous quorum sensing threshold function depending on bacterial concentration, the vector field switches when P crosses the threshold P_a. Therefore, perturbing a single parameter is insufficient to fully characterize system (1) responses near the threshold. For this reason, Latin hypercube sampling is used for global sampling over given parameter intervals, and partial rank correlation coefficients (PRCCs) are combined to analyze the influence of each parameter on system (1) outputs. The main output indices are selected as the long-term average bacterial concentration, bacterial oscillation amplitude, proportion of time for which quorum sensing is

activated, and long-term average immune level, defined respectively by

$$\overline{P} = \frac{1}{T-T_0}\int_{T_0}^{T} P(t)\mathrm{d}t, \quad A_P = \max_{t\in[T_0,T]} P(t) - \min_{t\in[T_0,T]} P(t),$$
$$\Phi_{\mathrm{QS}} = \frac{1}{T-T_0}\int_{T_0}^{T} I(P(t) > P_a)\mathrm{d}t, \quad \overline{B} = \frac{1}{T-T_0}\int_{T_0}^{T} B(t)\mathrm{d}t.$$

Here T_0 denotes the starting time after the transient is removed, and I is the indicator function. In this case, $T_0 = 0$ and $T = 500$. The quantity $\overline{P}$ characterizes the long term bacterial load level; A_P measures the intensity of periodic oscillations induced by Hopf bifurcation or threshold switching; Φ_{QS} describes the fraction of time for which the system (1) remains in the quorum sensing activated state; and $\overline{B}$ reflects the long term response level of the host immune system.

To further quantify the effect of different parameters on system (1) outputs, Figure 7 gives the PRCC results and bootstrap confidence intervals of each parameter with respect to $\overline{P}$, A_P, Φ_{QS}, and $\overline{B}$.



(a) (b) (c) (d)

Figure 7: Global parameter sensitivity analysis based on PRCC. (a) Sensitivity of each parameter to the long-term average bacterial concentration $\overline{P}$; (b) sensitivity of each parameter to bacterial oscillation amplitude A_P; (c) sensitivity of each parameter to the proportion of QS activation time Φ_{QS}; (d) sensitivity of each parameter to the long term average immune level $\overline{B}$. The asterisk indicates the significance level.

Figure 7 shows that: (1) for the long-term average bacterial concentration $\bar{P}$, the bacterial intrinsic growth rate r, the environmental carrying capacity K, and the QS intensity η are positively correlated with it, whereas the QS threshold P_a and the immune clearance rate δ are negatively correlated with it. (2) For the bacterial population oscillation amplitude A_P, the immune clearance rate δ exerts a positive effect, whereas P_a and d_0 exert negative effects.

(3) For the proportion of time during which quorum sensing is activated Φ_{QS}, parameters such as the QS intensity η are positively correlated with it, making the system more likely to remain in the QS activated state, whereas P_a and δ exhibit significant negative correlations with it. (4) For the long term average immune level $\bar{B}$, it increases with enhanced bacterial burden and inflammatory stimulation. However, when δ increases and effectively reduces the bacterial load, the persistent stimulation imposed on the immune system is weakened, and thus the long term average immune level may also decrease.

Sensitivity analysis indicates that the long term evolutionary outcome of *Pseudomonas aeruginosa* infection is jointly regulated by bacterial proliferative capacity, QS feedback intensity, the QS threshold, and immune clearance capacity. Higher values of r, K, and η promote the bacterial population to cross the threshold and maintain a high bacterial load state or periodic oscillations, thereby serving as important factors contributing to infection persistence and chronicity. In contrast, an increase in δ can reduce the bacterial burden and alleviate sustained immune stimulation. Therefore, the control of *Pseudomonas aeruginosa* infection should focus on combined regulation: on the one hand, suppressing bacterial proliferation and QS signal feedback, and on the other hand, enhancing B cell mediated clearance. Such regulation may drive the system from a high bacterial load or recurrent oscillatory state toward a stable state characterized by low bacterial burden and low immune stimulation, thereby reducing the risk of chronic infection maintenance and recurrence.

7 Conclusions

This article established and analyzed a four-dimensional discontinuous Filippov dynamical model and proves the non-negativity and boundedness of its solutions. The existence conditions and stability criteria are established for the disease free equilibrium, the low bacterial load positive equilibrium, the high bacterial load positive equilibrium, and the pseudo equilibrium on the switching manifold. Furthermore, the results show that the system may exhibit bistable dynamical behavior under certain parameter conditions. Taking the intrinsic growth rate of bacteria as the bifurcation parameter, this study derives the conditions for Hopf bifurcation near the positive equilibrium and determines the bifurcation type and the stability of periodic solutions by means of the first Lyapunov coefficient. Moreover, by choosing the natural decay rate of B cells as the second bifurcation parameter, the Bautin bifurcation in the degenerate Hopf case is investigated, and the criteria for the emergence of one or two small-amplitude limit cycles as well as a multiple limit cycle near the Bautin bifurcation point are obtained. These results theoretically demonstrate that quorum sensing threshold regulation may induce complex periodic oscillations and multiple limit cycle structures. Numerical simulations verify the theoretical results concerning the existence and stability of the equilibria, as well as the Hopf–Bautin bifurcation conditions. Finally, sensitivity analysis shows that enhanced immune clearance contributes to bacterial eradication and suppresses

both bacterial population oscillations and quorum sensing. Overall, this study provides a theoretical reference for understanding the interaction mechanism between bacterial populations and the human immune system under quorum sensing regulation in *Pseudomonas aeruginosa*, and offers numerical support for the investigation of anti quorum sensing therapy and immune regulation strategies.

Competing interests

The authors declare that they have no known competing financial interests or personal relationships that could have appeared to influence the work reported in this paper.

Data Availability

This study is based on theoretical mathematical analysis and numerical simulation, and no experimental data, clinical data, or externally collected datasets were used. All numerical results were generated by the four-dimensional Filippov dynamical system established in this paper; the model equations, parameter settings, and theoretical conditions are all given in the article. The numerical simulations are used mainly to investigate the stability of equilibria, sliding dynamics, Hopf bifurcation and Bautin bifurcation, and the existence of multiple limit cycles.

In addition, global sensitivity analysis was carried out using Latin hypercube sampling (LHS) and partial rank correlation coefficient (PRCC), and parameter sensitivity was evaluated through bootstrap confidence intervals. The corresponding simulation data were generated by varying the model parameters and computing four output measures: the long-term average bacterial concentration, the amplitude of bacterial oscillations, the proportion of time during which quorum sensing is activated, and the long-term average immune response level.

All results of this study originate from the mathematical model and the numerical computation procedure described in the paper, and do not depend on any independent empirical dataset. The corresponding numerical data can be reproduced from the governing equations, parameter values, and computational methods provided in the article.

References

[1] S. T. Rutherford and B. L. Bassler, "Bacterial quorum sensing: Its role in virulence and possibilities for its control," *Cold Spring Harbor Perspectives in Medicine*, vol. 2, Art. no. a012427, 2012.

[2] P. N. Jiménez, G. Koch, J. A. Thompson, *et al.*, "The multiple signaling systems regulating virulence in *Pseudomonas aeruginosa*," *Microbiology and Molecular Biology Reviews*, vol. 76, pp. 46–65, 2012.

[3] R. Medzhitov, "Inflammation 2010: New adventures of an old flame," *Cell*, vol. 140, pp. 771–776, 2010.

[4] A. Abu Khweek and A. O. Amer, "Adaptive immunity to *Pseudomonas aeruginosa*," *Immunological Research*, vol. 2018, Art. no. 2490690, 2018.

[5] G. Telford, D. Wheeler, P. Williams, *et al.*, "The *Pseudomonas aeruginosa* quorum sensing signal molecule N-(3-oxododecanoyl)-L-homoserine lactone has immunomodulatory activity," *Infection and Immunity*, vol. 66, no. 1, pp. 36–42, 1998.

[6] R. S. Smith, S. G. Harris, R. Phipps, *et al.*, "The *Pseudomonas aeruginosa* quorum sensing molecule N-(3-oxododecanoyl)homoserine lactone contributes to virulence and induces inflammation in vivo," *Journal of Bacteriology*, vol. 184, no. 4, pp. 1132–1139, 2002.

[7] D. Bortolotti, J. LeMaoult, C. Trapella, *et al.*, "*Pseudomonas aeruginosa* quorum sensing molecule N-(3-oxododecanoyl)-L-homoserine lactone induces HLA-G expression in human immune cells," *Infection and Immunity*, vol. 83, no. 10, pp. 3918–3925, 2015.

[8] P. Fergola, J. Zhang, M. Cerasuolo, *et al.*, "On the influence of quorum sensing in the competition between bacteria and immune system of invertebrates," in *AIP Conference Proceedings*, vol. 1028. Melville, NY, USA: American Institute of Physics, 2008, pp. 215–232.

[9] A. J. Koerber, J. R. King, J. P. Ward, *et al.*, "A mathematical model of partial-thickness burn-wound infection by *Pseudomonas aeruginosa*: Quorum sensing and the build-up to invasion," *Bulletin of Mathematical Biology*, vol. 64, no. 2, pp. 239–259, 2002.

[10] J. P. Ward, J. R. King, A. J. Koerber, *et al.*, "Mathematical modelling of quorum sensing in bacteria," *IMA Journal of Mathematics Applied in Medicine and Biology*, vol. 18, no. 3, pp. 263–292, 2001.

[11] Z. H. Zhang, Y. H. Suo, J. G. Peng, *et al.*, "Analysis of a periodic bacteria-immunity model with delayed quorum sensing," *Computers & Mathematics with Applications*, vol. 56, no. 11, pp. 2834–2847, 2008.

[12] A. Wang and Y. Xiao, "A Filippov system describing media effects on the spread of infectious diseases," *Nonlinear Analysis: Hybrid Systems*, vol. 11, pp. 84–97, 2014.

[13] Z. Guo, L. Huang, and X. Zou, "Impact of discontinuous treatments on disease dynamics in an SIR epidemic model," *Mathematical Biosciences and Engineering*, vol. 9, no. 1, pp. 97–110, 2012.

[14] W. Qin and S. Tang, "The selection pressures induced non-smooth infectious disease model and bifurcation analysis," *Chaos, Solitons & Fractals*, vol. 69, pp. 160–171, 2014.

[15] N. S. Chong, B. Dionne, and R. Smith, "Modelling avian influenza using Filippov systems to determine culling of infected birds and quarantine," *Nonlinear Analysis: Real World Applications*, vol. 24, pp. 196–218, 2015.

[16] T. Carvalho, R. Cristiano, D. S. Rodrigues, *et al.*, "Global analysis of a piecewise smooth epidemiological model of COVID-19," *Nonlinear Dynamics*, vol. 105, no. 4, pp. 3763–3773, 2021.

[17] C. Chen, N. S. Chong, and R. Smith, "A Filippov model describing the effects of media coverage and quarantine on the spread of human influenza," *Mathematical Biosciences*, vol. 296, pp. 98–112, 2018.

[18] Y. Zhang and Y. Xiao, "Global dynamics for a Filippov epidemic system with imperfect vaccination," *Nonlinear Analysis: Hybrid Systems*, vol. 38, Art. no. 100932, 2020.

[19] C. Dong, C. Xiang, Z. Xiang, *et al.*, "Global dynamics of a Filippov epidemic system with nonlinear thresholds," *Chaos, Solitons & Fractals*, vol. 163, Art. no. 112560, 2022.

[20] H. Zhou and S. Tang, "Bifurcation dynamics on the sliding vector field of a Filippov ecological system," *Applied Mathematics and Computation*, vol. 424, Art. no. 127052, 2022.

[21] C. Dong, L. Zhang, and Z. Teng, "Stability and bifurcations for a 3D Filippov SEIS model with limited medical resources," *Advances in Continuous and Discrete Models*, vol. 2024, Art. no. 39, 2024.

[22] M. Flückiger, M. Ludwig, and A. S. Önder, "Ebola and state legitimacy," *The Economic Journal*, vol. 129, no. 621, pp. 2064–2089, 2019, doi: 10.1111/ecoj.12638.

[23] B. D. Hassard, N. D. Kazarinoff, and Y. H. Wan, *Theory and Applications of Hopf Bifurcation*. Cambridge, U.K.: Cambridge University Press, 1981.

[24] J. Guckenheimer and P. Holmes, *Nonlinear Oscillations, Dynamical Systems, and Bifurcations of Vector Fields*. New York, NY, USA: Springer, 1983.

[25] S. N. Chow, C. Li, and D. Wang, *Normal Forms and Bifurcation of Planar Vector Fields*. Cambridge, U.K.: Cambridge University Press, 1994.

[26] Y. Guo and B. Niu, "Bautin bifurcation in delayed reaction-diffusion systems with application to the Segel-Jackson model," *Discrete and Continuous Dynamical Systems–Series B*, vol. 24, no. 11, pp. 6005–6024, 2019.

[27] N. N. Bautin, "On the number of limit cycles which appear with the variation of coef-

ficients from an equilibrium state of the type focus or center," *American Mathematical Society Translations*, vol. 100, pp. 1–19, 1954. Original work published in *Matematicheskii Sbornik*, vol. 30, no. 72, pp. 181–196, 1952.

[28] C. J. Silva, G. Cantin, C. Cruz, *et al.*, "Complex network model for COVID-19: Human behavior, pseudo-periodic solutions and multiple epidemic waves," *Journal of Mathematical Analysis and Applications*, vol. 514, no. 2, Art. no. 125171, 2022.

[29] W. Zhou, T. Zhao, A. Wang, *et al.*, "Bifurcations and dynamics of a Filippov epidemic model with nonlinear threshold control policy and medical-resource constraints," *Chaos, Solitons & Fractals*, vol. 184, Art. no. 114992, 2024.

[30] S. Qin, W. Xiao, C. Zhou, *et al.*, "*Pseudomonas aeruginosa*: Pathogenesis, virulence factors, antibiotic resistance, interaction with host, technology advances and emerging therapeutics," *Signal Transduction and Targeted Therapy*, vol. 7, Art. no. 199, 2022.

[31] S. W. Miranda, K. L. Asfahl, A. A. Dandekar, *et al.*, "*Pseudomonas aeruginosa* quorum sensing," *Advances in Experimental Medicine and Biology*, vol. 1386, pp. 95–115, 2022.

[32] Y. Lu, Y. Lv, S. Niu, *et al.*, "Quorum sensing regulates heteroresistance in *Pseudomonas aeruginosa*," *Frontiers in Microbiology*, vol. 13, Art. no. 1017707, 2022.

[33] R. Yin, J. Cheng, J. Wang, *et al.*, "Treatment of *Pseudomonas aeruginosa* infectious biofilms: Challenges and strategies," *Frontiers in Microbiology*, vol. 13, Art. no. 955286, 2022.

[34] M. Chen, J. Ji, H. Liu, *et al.*, "Periodic oscillations in the quorum sensing system with time delay," *International Journal of Bifurcation and Chaos*, vol. 30, no. 9, Art. no. 2050127, 2020.

[35] M. Cerasuolo, "On the influence of diffusion on the competition between bacteria and innate immune system of invertebrates," *Ricerche di Matematica*, vol. 59, pp. 165–185, 2010.

[36] A. R. M. Almeida, I. F. Amado, J. Reynolds, *et al.*, "Quorum-sensing in CD4+ T cell homeostasis: A hypothesis and a model," *Frontiers in Immunology*, vol. 3, Art. no. 125, 2012.

[37] J. Reynolds, I. F. Amado, A. A. Freitas, *et al.*, "A mathematical perspective on CD4+ T cell quorum sensing," *Journal of Theoretical Biology*, vol. 347, pp. 160–175, 2014.

[38] E. C. Schrom II, S. A. Levin, and A. L. Graham, "Quorum sensing via dynamic cytokine signaling comprehensively explains divergent patterns of effector choice among helper T cells," *PLoS Computational Biology*, vol. 16, no. 7, Art. no. e1008051, 2020.

[39] H. K. Khalil, *Nonlinear Systems*, 3rd ed. Upper Saddle River, NJ, USA: Prentice Hall, 2002.

[40] W. Govaerts, Y. A. Kuznetsov, and B. Sijnave, "Numerical methods for the generalized Hopf bifurcation," *SIAM Journal on Numerical Analysis*, vol. 38, no. 1, pp. 329–346, 2000.